ENTEROVIRUS LOCALIZATION IN THE SPLEEN - DETECTION OF MULTIPLE TARGETS WITHIN A SINGLE TISSUE SECTION

Master's thesis
Johannes Malkamäki
Tampere University
Faculty of Medicine and Health Technology
24.04.2019

PRO GRADU -TUTKIELMA

Paikka:	Tampereen yliopisto Lääketieteen ja terveysteknologian tiedekunta
Tekijä:	Malkamäki, Johannes Juuso Aleksi
Otsikko:	Enteroviruksien sijainnit pernassa – Monien markkerien havaitseminen
yhdestä kudosleikkeestä	
Sivut:	64 s.
Ohjaaja:	FT Jutta Laiho
Tarkastajat:	FT Jutta Laiho ja apulaisprofessori Vesa Hytönen
Aika:	24.04.2019

Tiivistelmä

Tutkielman tausta ja tavoitteet: Immunofluoresenssivärjäyksessä käytetään fluoresoivia vasta-aineita antigeenien värjäämiseen. Fluoresoivat vasta-aineet voidaan pestä pois kudokselta eluutioliuoksilla kudoksen kuvantamisen jälkeen. Tämä mahdollistaa kudoksen peräkkäisen värjäämisen monien vasta-aineiden avulla. Kokonainen kudosleike voidaan kuvantaa modernilla virtuaalimikroskooppijärjestelmällä, ja peräjälkeen värjätyn kudosleikkeen kuvat voidaan yhdistää yhdeksi kuvaksi, joka ilmentää monia kudosmarkkereita. Yksi tämän tutkimuksen tavoitteista oli pystyttää eluutio- ja kuvantamisprotokolla, jonka avulla pystyttäisiin peräjälkeen värjäämään pernanäytteitä. Kun tämä protokolla oli pystytetty, pernanäytteitä tyypin 1 diabeetikoilta, tyypin 1 diabeteksen kaltaisilta autovasta-aine positiivisilta potilailta ja kontrolleilta pystyttiin värjäämään. Pernakudosta värjättiin enterovirusvasta-aineella ja pernan lymfosyyttivasta-aineilla ja näiden kolokalisaatiota tutkittiin.

Materiaalit ja menetelmät: Eluutio- ja kuvantamisprotokolla pystytettiin käyttämällä elinluovuttajien pernanäytteitä. Kudosnäytteitä värjättiin enterovirusvasta-aineella ja monilla lymfosyyttivasta-aineilla. Vasta-aineiden värjäämistä testattiin sekä yksinkertaisilla että monivärjäysmenetelmillä. Monivärjäysmenetelmää testattiin vasta-aine-cocktail-protokollalla ja Fab-fragmentilla, joka estää vasta-aineen epäspesifisen sitoutumisen värjäysten välissä. Vasta-aineiden eluutiota testattiin SDS pH2 liuoksella ja 2-ME/SDS liuoksella. Leikkeiden kuvantaminen tehtiin Slidestrider -virtuaalimikroskopiajärjestelmällä. Kun eluutio- ja kuvantamisprotokolla oli pystytetty, optimoiduilla vasta-aineilla värjättiin pernanäytteitä tyypin 1 diabeetikoilta, tyypin 1 diabetekseen liittyviltä autovasta-aine positiivisilta henkilöiltä ja kontrolleilta.

Tulokset: Vasta-aine -cocktail-protokolla ja Fab-fragmentilla blokkaaminen osoittautuivat toimimattomiksi värjäysmenetelmiksi tätä työtä varten, ja värjäykset päädyttiin tekemään yksinkertaisella menetelmällä. 2-ME/SDS osoittautui toimivaksi eluutioliuokseksi kaikille testatuille vasta-aineille, ja sitä käytettiin lopullisessa värjäysprotokollassa pernanäyteille. Slidestrider -virtuaalimikroskopiajärjestelmä osoittautui haasteelliseksi, ja sen takia ainoastaan enteroviruspositiiviset kohdat kudoksilta kuvannettiin. Eri markkereilla otetut kuvat yhdistettiin yhdeksi kuvaksi ja huomattiin enteroviruksen kolokalisoituvan eniten CD3 (T-solu) ja CD68 (makrofagi) markkerien kanssa.

Johtopäätökset: Toimiva eluutio- ja kuvantamisprotokolla saatiin pystytettyä, mikä säästää arvokasta kudosmateriaalia mahdollistaen useamman markkerin analysoinnin yhdestä ja samasta kudosleikkeestä. Pernanäytteiltä löytyi enteroviruspositiivisia soluja ja kolokalisaatiota useamman testatun markkerin kanssa. Pystytettyä eluutioprotokollaa voidaan käyttää myös muiden kudosten värjäämisessä. Kuvantamismenetelmä osoittautui käytetyllä laitteistolla haasteelliseksi, minkä vuoksi jatkossa muita olemassa olevia laitteistoja on syytä harkita.

MASTER'S THESIS

Place:	Tampere University Faculty of Medicine and Health Technology
Author:	Malkamäki, Johannes Juuso Aleksi
Title:	Enterovirus localization in the spleen – Detection of multiple targets within a single tissue section
Pages:	64 p.
Supervisor:	PhD Jutta Laiho
Reviewers:	PhD Jutta Laiho and associate professor Vesa Hytönen
Date:	24.04.2019

Abstract

Background and aims: In immunofluorescence staining, fluorescently tagged antibodies are used to target antigens. Antibodies stained using immunofluorescence can be washed off the tissue using elution buffers after imaging the sample. This makes possible the consecutive staining of a sample with multiple markers. The whole slide imaging of a tissue sample is possible with a modern virtual microscopy system. Consecutively stained tissue samples can be imaged using a virtual microscope tissue scanner and the images taken can be combined into one image displaying multiple markers. One of the aims of this study was to set up an elution and imaging workflow for the consecutive staining of spleen tissue samples. With this workflow in place, spleen tissue samples from type 1 diabetics, type 1 diabetes -related autoantibody-positive patients and control donors were analyzed for enterovirus positivity and enterovirus colocalization with splenic lymphocyte markers.

Materials and methods: The elution and imaging workflow was set up using spleen samples from organ donors. The samples were stained with an anti-enterovirus marker and several lymphocyte markers. Antibodies were tested with both a single staining and multiple staining protocols. The multiple staining of antibodies was tested with an antibody cocktail and using a Fab-fragment as a blocking step in between stains. The elution of antibodies was tested with an SDS pH2 solution and a 2-ME/SDS solution. The imaging of samples was done with the Slidestrider virtual microscopy system. With the ready elution and imaging workflow, spleen samples from type 1 diabetics, type 1 diabetes -related autoantibody-positive patients and control donors samples were stained with optimal antibody concentrations and imaged.

Results: The cocktail and Fab fragment double staining methods did not prove effective for this study, and stainings were done with one antibody at a time. 2-ME/SDS was an effective elution solution for all tested antibodies, and it was used as the elution solution in the final staining of spleen samples. Due to difficulties with the Slidestrider virtual microscopy system, only the enterovirus-positive sites on the samples were imaged. The images for the different markers were then combined, and the enterovirus-positive sites were observed to colocalize most with the CD3 (T cell) and the CD68 (macrophage) markers.

Conclusions: The elution and imaging workflow was successfully set up, saving precious sample material and facilitating the staining of multiple markers on the same tissue sample. The spleen samples were enterovirus positive and the positivity colocalized with multiple markers. The protocol set up in this study can be used for staining other tissue samples. The imaging system proved challenging for executing the imaging workflow, and other imaging systems should be considered for future stainings.

Acknowledgements

This thesis work was carried out in the Virology group in the Faculty of Medicine and Life Sciences at the Tampere University between June 2017 and January 2018. This work is only possible because of the enthusiastic and supportive environment of the Virology group. It has been my absolute privilege to be part of this community searching for answers to fundamental questions about human disease. This work would not have been possible without the following people.

Establishing the protocols of the lab work for this study has been only been possible with the aid of the laboratory technician Sari Toivola. Sari's far-reaching skill set in tissue staining has helped overcome many difficulties faced in this work. Technicians Eeva Tolvanen and Minta Lumme were also very helpful, providing a helping hand and useful suggestions for lab work. Thank you, Sari, Eeva, and Minta.

The imaging of tissue samples was possible with the equipment of the histology core of Tampere University. I want to thank Onni Ylinen from Jilab, who provided considerable and regular support for the use of the virtual microscopy system. Onni was also key in scripting the programs for slide recognition and stacking of whole slide tissue scans. I would also like to thank the professor of cancer biology, Jorma Isola, for providing assistance with tissue scanning and tips in tissue staining.

A big thanks goes to professor of virology and virology group leader Heikki Hyöty for encouraging this research and providing an environment where curiosity and scientific ambition thrives. I strongly believe that Heikki's group is a place from where excellent science stems.

Finally, this thesis work would not have been possible without the continuous support of my instructor PhD Jutta Laiho, whose expertise has been invaluable for the completion of both the lab work and the writing of this thesis. Not only has Jutta's scientific knowledge been very helpful, but she has also assisted with the lab work and in the crafting of this written work. A major part of this thesis work was setting up new protocols for staining, and throwing around ideas with Jutta has been a very productive and fun part of this work. Jutta has also been a crucial support during the many unexpected difficulties facing this work. Thank you, Jutta, with your guidance I have grown much as a scientist.

Lastly, I would like to thank my girlfriend Lotta from the bottom of my heart for supporting me throughout this work. Without your continuous positive energy and patience, this thesis work would not have completed.

Abbreviations

2-ME	2-Mercaptoethanol
A549	Adenocarcinomic human alveolar basal epithelial cell
AAb+	Type 1 diabetes -related autoantibody-positive patients
BABYDIET	The Primary dietary intervention study to reduce the risk of islet autoimmunity in children at increased risk for type 1 diabetes
CV-A	Coxsackie A virus
CV-B	Coxsackie B virus
CV-B1	Coxackie B virus 1
DAB	3,3'-diaminobenzidine
DAPI	4',6-diamidino-2-phenylindole
ddH_2O	Double-distilled water
DIPP	The Finnish Type 1 Diabetes Prediction and Prevention study
DiViD	The Diabetes Virus Detection study
EDTA	Ethylenediaminetetraacetic acid
eIF4G	cellular translation initiation factor 4 gamma 1
EV	Enterovirus
Fab	Antigen-binding fragment
FFPE	Formalin-fixed paraffin-embedded
HCl	Hydrogen chloride
HIER	Heat-induced antigen retrieval
HLA	Human leukocyte antigen
HRP	Horse radish peroxidase
IF	Immunofluorescence
IgG	Immunoglobulin G
IgM	Immunoglobulin M
IHC	Immunohistochemistry
KCL	Potassium chloride
nPOD	The Network for Pancreatic Organ donors with Diabetes
PALS	Perilymphatic region
PBS	Phosphate-buffered saline
PEVNET	The Persistent Virus Infection in Diabetes Network
PLN	Pancreatic lymph node
PKR	Protein kinase R
SDS	Sodium dodecyl sulphate
T1D	Type 1 diabetes
TEDDY	The Environmental Determinants of Diabetes in the Young study
TRIGR	The Trial to Reduce IDDM in the Genetically at Risk study
Tris	Tris(hydroxymethyl)aminomethane
UTR	Untranslated region
VP1	Enteroviral protein 1
VP2	Enteroviral protein 2
VP3	Enteroviral protein 3
VP4	Enteroviral protein 4
VPg	Genome-linked viral protein

Table of Contents

1 Introduction

The emergence of virtual microscopy whole slide imaging systems (Rojo et al., 2006) and the development of antibody elution protocols (Gendusa et al., 2014) are opening up the possibility of staining entire tissue samples with multiplexing strategies. Virtual microscopy creates a large image of the whole tissue sample storing the information of the staining in a digital format (Higgins, 2015). The information on the sample is protected even if the slide breaks (Camparo et al., 2012). Having a digital copy of the slide also allows the comparison of data from different stainings (Bolognesi et al., 2017) and the analysis of the staining with algorithms (Ghaznavi et al., 2013).

With fluorescent stainings, the multiplexing of tissue markers is possible, and colocalization studies of the markers can be made (Bolte & Cordelières, 2006). Unlike most chromogenic stains, fluorescent markers don't attach to the sample covalently (Burry, 2010c). This makes the elution of fluorescent markers form tissue samples possible (Gendusa et al., 2014), much like in Western blot, where removal of the bound antibody has been used for a longer time (Kaufmann et al., 1987). Combining the information from multiple fluorescent markers on a tissue-wide scale can provide a large pool of data from precious tissue samples (Bolognesi et al., 2017).

Enteroviruses (EV) have been associated with type 1 diabetes (T1D) in many epidemiological studies (Hyöty, 2016; Yeung et al., 2011). EVs have also been found in tissues of T1D patients, especially in the pancreas and small intestine (Dotta et al., 2007; Krogvold et al., 2015; M. Oikarinen et al., 2018, 2012; Richardson et al., 2009). To date, the EV positivity in the spleen of T1D patients has not been studied extensively. Tissue banks providing tissue samples from T1D donors have been scarce. However, the creation of a U.S. based Juvenile Diabetes Research Foundation (JDRF) -funded network for Pancreatic Organ Donors with Diabetes (nPOD) tissue bank (Pugliese et al., 2014), has enabled further T1D-related tissue studies to be performed in different international laboratories. nPOD collects tissues such as pancreas, duodenum, and spleen from brain-dead organ donors with T1D, donors with T1D-related autoantibodies without disease and from non-diabetic donors.

Studying EV positivity in tissue samples is challenging without the use of virtual microscopy and scanning of the stained slides. As tissue samples from T1D donors are precious, it is beneficial to use one single tissue section for staining multiple markers. This can be done by eluting first stained markers and subsequently staining with other markers. Locating individual EV-positive

cells in large tissue samples is laborious and relocating those same locations after the removal of the anti-EV antibody and the staining of another tissue marker becomes almost impossible. Utilizing the virtual microscopy systems for whole slide scanning in combination with fluorescent multiplexing provides a novel way to study the localization of enterovirus positivity in a tissue-wide scale.

With few prior studies of the EV positivity in T1D patient's spleens and the availability of spleen samples, in combination with the unique study design, makes an interesting starting point for this study.

2 Review of the literature

2.1 Immunohistochemical staining

2.1.1 Chromogenic and immunofluorescent staining methods

Immunodetection of antigens on tissue samples is a standard diagnostic tool for pathologists and is widely used in research as well. The ability to pinpoint the location of an antigen within a cell or tissue sample is a unique property of immunohistochemical methods not available to other biochemical assays (José A. Ramos-Vara, 2011). The detection of antigens on the tissue requires a labelled antibody. Antibodies can be labelled in three ways: with an enzyme producing a precipitate on around the antigen, with a fluorophore that signals under laser excitation or with a particulate like gold or silver (Burry, 2010c). Many detection methods have been developed with varying sensitivities. The more complex the detection method, the more sensitive the staining method usually is (José A. Ramos-Vara, 2011).

In enzymatic detection, an enzymatic reaction occurs at the site of antibody binding to the antigen. The reaction is caused by horseradish peroxidase (HRP) or a similar enzyme, and the reaction product is a colored substance such as oxidized 3,3'-diaminobenzidine (DAB) that covalently binds to the tissue around the antibody (Fig. 1). IHC staining methods that leave a substrate covalently conjugated to the tissue are called chromogenic detection methods. Chromogenic methods give a strong signal since the enzymatic reaction can significantly amplify the signal of even a small amount of target bound antibody. However, the chromogenic signal can be somewhat diffuse when compared to a fluorescent signal, since the enzymatic precipitate can diffuse slightly from the antibody binding site. Chromogenically stained samples can be viewed with a brightfield microscope. (Burry, 2010c)

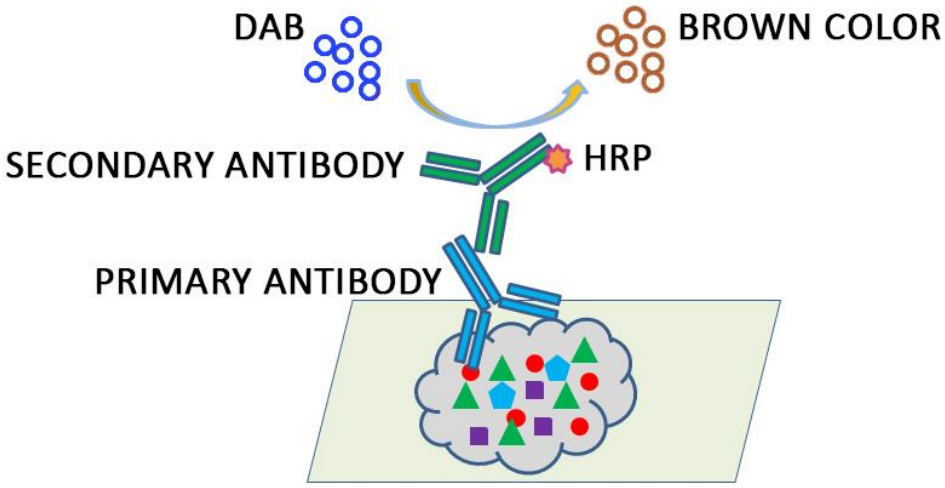

Figure 1. The amplification of the signal of an antigen-bound antibody by the enzymatic horseradish peroxidase (HRP) method. A secondary antibody attached to HRP recognizes the primary antigen-bound antibody. When diaminobenzidine (DAB) is added to the tissue with hydrogen peroxide present, a colored substance is produced that covalently links to the tissue staining it. Image adapted from an image by Sino Biological (http://www.sinobiological.com/immunohistochemical-ihc-introduction.html 17.04.2019).

The other common detection method for protein antigens is immunofluorescence (IF), where detection happens via a fluorophore-bound antibody (Fig. 2). In direct detection, the fluorophore is directly attached to the primary antibody that recognizes the target antigen in the tissue (Coons et al., 1941). In indirect detection, however, the fluorophore is attached to a secondary antibody that recognizes the primary antibody (Coons et al., 1955).

Although having the fluorophore attached to the secondary antibody makes the staining process more laborious, it has advantages: Firstly, the signal of the bound primary antibody is amplified since many secondary antibodies with fluorophores can attach to a single primary antibody (Buchwalow & Böcker, 2010d). Secondly, each primary antibody does not need to be conjugated to a fluorophore. Instead, one secondary fluorophore-conjugated antibody can be used in several stainings to recognize different primary antibodies (Burry, 2010a). Then again, using a direct detection method is less prone to false positive signal, since no secondary antibody could cross-react with other bound antibodies or bind non-specifically to the tissue (Buchwalow & Böcker, 2010d). Using the direct method also facilitates the staining of multiple markers simultaneously, even when the antibodies are raised in the same species (Buchwalow & Böcker, 2010b).

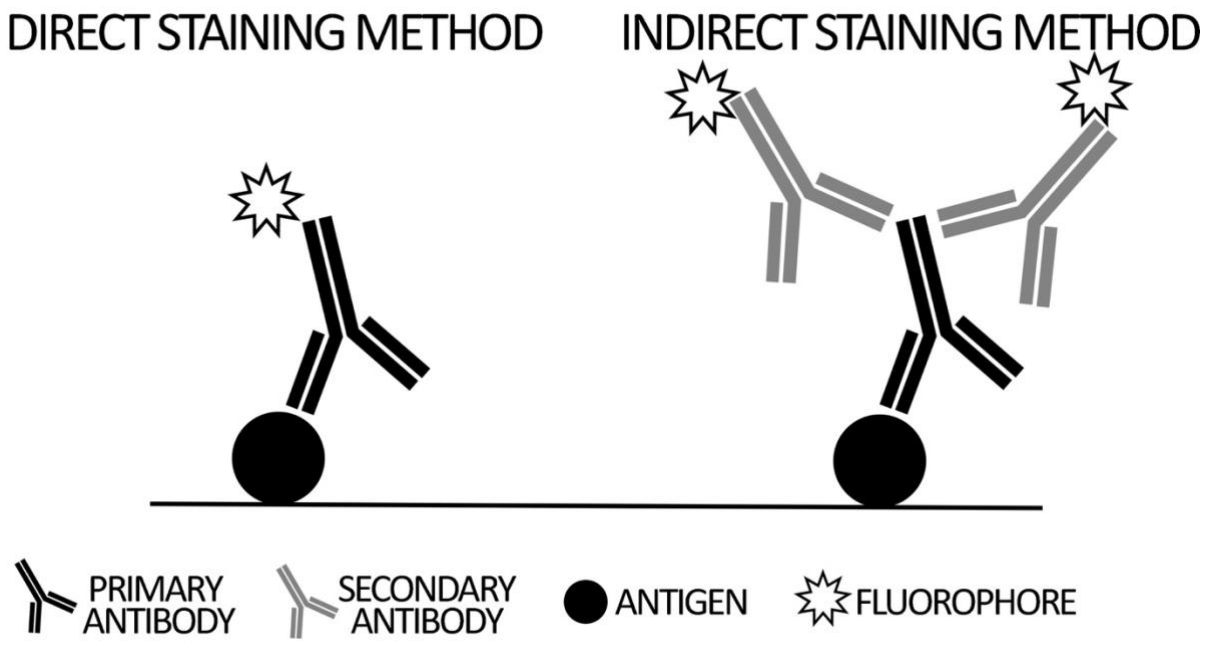

Figure 2. The difference between direct in indirect immunofluorescent staining. In the left image, the fluorophore is attached to the primary antibody, which binds to the antigen on the cell. In the right image, the antigen-bound primary antibody does not a have fluorophore attached to it but instead is bound by secondary antibodies attached to a fluorophore.

2.1.2 Immunofluorescent staining with multiple antibodies

Staining multiple markers simultaneously saves reagents and time. It also allows more information to be gained from the sample since the expression and localization of these markers can be visualized on one single section (Buchwalow & Böcker, 2010c). Having two or more signals on the sample also saves time when imaging, since a virtual microscopy system can easily switch between channels and rescan the sample for a second or a third signal.

Chromogenic stainings are widely used as diagnostic stains by pathologists as the signal is strong and easily viewed with a light microscope. Nevertheless, chromogenic stains have critical drawbacks when compared to fluorescent staining: Chromogenic staining is not suitable for studying antigens that are near each other for example within the nucleus (José A. Ramos-Vara, 2011). Most chromogenic staining methods leave a covalently bound colored precipitate on the tissue that blocks the binding of subsequent antibodies (Valnes & Brandtzaeg, 1984). An exception is 3-Amino-9-ethyl carbazole (AEC) that is alcohol soluble and can be washed from the slide (Gendusa et al., 2014). Therefore, attention must be paid when staining for multiple markers with a chromogenic stain.

In contrast to chromogenic staining, in fluorescent staining, the attachment of an antibody to the target antigen does not block the binding of other antibodies nearby (Buchwalow & Böcker, 2010b). This can be utilized in double or triple stainings, where multiple primary antibodies are incubated on the sample simultaneously with secondary antibodies (Buchwalow & Böcker, 2010b). In optimal conditions, multiple signals can be detected from the sample with appropriate filter cubes (Buchwalow & Böcker, 2010a). Using multiple antibodies enables signal colocalization studies, where the overlapping signals can be assessed (Bolte & Cordelières, 2006). Since the bound primary and secondary antibodies are not covalently attached to the tissue in fluorescent stainings, washing the antibodies off the tissue is possible, and consequent stainings on the same sample can be performed (Pirici et al., 2009).

When staining for multiple antibodies simultaneously with the antibody cocktail method, great attention should be paid to selecting appropriate antibodies. Antibodies should have either been raised in different species or they should be of a different isotype, to avoid cross-recognition by the secondary antibodies. (Buchwalow & Böcker, 2010b)

Attention should also be paid to the emission spectra of the secondary antibodies' fluorophores and the filter set of the microscope. The chosen fluorophores emission spectra should match the filter set of the microscope. If multiple markers are stained for with multiple fluorophores, narrow-band filter cubes need to be used to distinguish the emission spectra from one another. (Buchwalow & Böcker, 2010a)

2.1.3 Staining for multiple antibodies simultaneously using the Fab-fragment

With most monoclonal antibodies raised in mice (J. A. Ramos-Vara, 2005), the utilization of indirect immunofluorescent cocktail stainings can be tricky. Staining with antibodies raised in the same species and with the same antibody isotype causes cross-reactions between the bound first secondary antibody and the unbound second primary antibody since the first secondary antibody has free binding sites (Negoescu et al., 1994). Cross-reactions also happen between the second secondary antibody and the first primary antibody, since the first primary antibody is not saturated with the first secondary antibody (Negoescu et al., 1994).

One way to overcome this issue is to change the species of the first primary antibody to another with a Fab-fragment and then continue staining with another primary antibody. The Fab-fragment binds to the first primary antibody and coats it (Fig. 3). Next, a secondary antibody is added that recognizes the species the Fab-fragment was raised in. For example, a rabbit anti-human

primary antibody bound to its target is switched to a goat anti-human antibody by coating it with goat anti-rabbit monovalent polyclonal Fab-fragments. A donkey anti-goat secondary antibody is then used to recognize the bound Fab-fragment. Subsequently, the second primary antibody staining can be done with a rabbit anti-human antibody, which can be recognized with a donkey anti-mouse secondary antibody. This way no cross-reaction occurs and both secondary antibodies display the correct signal. (Franzusoff et al., 1991)

Staining with a Fab-fragment does make the protocol longer because the stains are not performed simultaneously and since an extra incubation step is needed for the Fab-fragment. The stains can still be performed within one protocol, saving time on common steps of the protocol that must be performed for each stain.

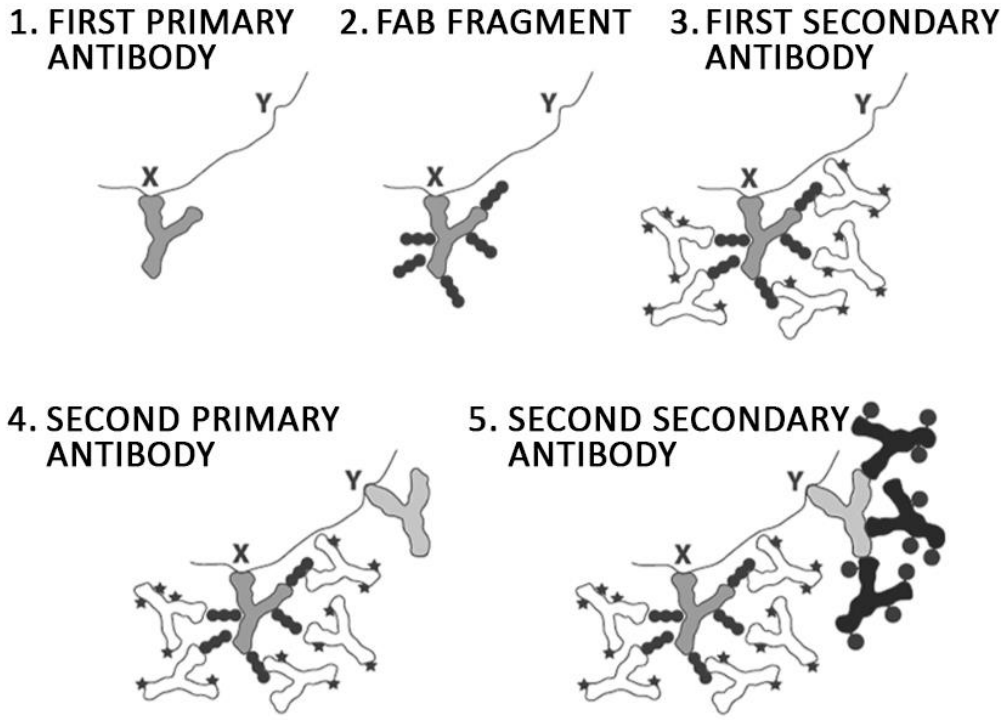

Figure 3. A method for using the Fab-fragment to stain for multiple antibodies from the same species. Both primary antibodies are raised in the same species. 1. The first primary antibody stained for binds to antigen X. 2. The first primary antibody is coated with a monovalent polyclonal Fab-fragment saturating the antibody. The Fab-fragment recognizes the species of the first primary antibody. 3. The first secondary antibody with a signal molecule attached binds to the Fab-fragments as it recognized the species of the Fab-fragments. 4. A second primary antibody binds to antigen Y. 5. The second secondary antibody with a different signal molecule attached binds to the second primary antibody. The second secondary antibody does not cross-react with the first primary antibody, because the first primary antibody is coated with the Fab-fragment. Image adapted from an image by Jackson ImmunoResearch (www.jacksonimmuno.com/technical/products/protocols/double-labeling-same-species-primary/example-b 20.01.2019).

2.2 Multiplexing or performing multiple stainings on the same sample

Standard practice for studying multiple antigens from tissue samples is to stain sequential sections with a single marker (Bolognesi et al., 2017). This method has obvious drawbacks; a lot of tissue is wasted to study multiple antigens and studying the colocalization of signals from the sequential sections is difficult (Bolognesi et al., 2017). In contrast, staining the same sample multiple times saves important tissue samples and allows for more data to be obtained (Gerdes et al., 2013). Multiplexing or performing multiple stainings on the same tissue sample has recently gained momentum (Bolognesi et al., 2017; Gerdes et al., 2013; Yarilin et al., 2015). Multiple stainings can be performed by photobleaching the existing fluorophores on the tissue, by blocking attached antibodies before restaining or by removing the attached antibodies before restaining (Bolognesi et al., 2017). Lately "next generation IHC" methods have also been developed, where either isotype-tagged antibodies or barcode labeled probes are used (Bolognesi et al., 2017).

Photobleaching fluorophores require primary antibody conjugated fluorophores to be used and have been used to stain up to 61 antigens on a sample (Gerdes et al., 2013). As reviewed above in "Chromogenic and immunofluorescence staining methods," staining with primary antibody conjugates has drawbacks. Blocking previously used antibodies can be done with a Fab-fragment solution or with chromogenic stains, but this also blocks other antigens nearby.

Several methods have been studied for stripping antibodies off the tissue. The methods include boiling the sample in antigen retrieval solution and incubating the sample in strong chemical agents, detergents, proteases and extreme acidic solutions (Bolognesi et al., 2017). Heating the sample to remove bound antibodies is ineffective since antibodies are able to withstand high temperatures (Wang et al., 2007). At least two antibody stripping methods have been reported as effective in the academic literature. One of the methods utilizes an SDS pH2 glycine solution and the other uses 2-mercaptoethanol SDS to strip antibodies (Gendusa et al., 2014; Pirici et al., 2009).

Pirici et al. describe an antibody stripping procedure using a glycine-SDS pH2 buffer (Pirici et al., 2009). They compared a number of antibody stripping solutions with high osmolarity, extreme pH and with denaturing qualities (glycine pH 10, glycine-SDS pH 2, glycine pH 2.2, 3.5M KCl, Tris-SDS pH 6.75, Tris-SDS B-mercaptoethanol pH 6.75) and conclude that glycine-SDS pH 2 stripping buffer is the only buffer that thoroughly removes all bound antibody. Pirici et al. applied the elution methods against 14 anti-human antibodies raised in both mouse and rabbit, and they report that the minimum elution time for the sample is 30 minutes at 50 °C with agitation. According to their observation, multiple antibody stripping rounds do not affect the antigenicity of the sample when

tested for several monoclonal and polyclonal antibodies. They also report that the samples remain attached to the slide after multiple rounds of antibody stripping.

Gendusa et al. conclude that 2-Mercaptoethanol/SDS (2-ME/SDS) is the stripping buffer that removes antibodies most effectively when compared to glycine-SDS pH 2 and 6M urea (Gendusa et al., 2014). Gendusa et al. performed the glycine-SDS pH 2 elution protocol as described by Pirici et al. and report that 2-ME/SDS is the only buffer that removed all bound antibodies from a pool of 31 mouse and rabbit anti-human antibodies. According to Gendusa et al., glycine-SDS pH 2 buffer was able to remove all bound primary antibody when no secondary antibody with a marker was attached. When a secondary antibody was bound to the primary antibody, the glycine-SDS pH 2 buffer could not remove the primary antibody with the highest affinity. They conclude that 2-ME/SDS is the most effective elution solution because it destroys the disulfide bond within the antibody. Gendusa et al. report that the antigenicity of the tissue is largely unaffected by repeated 2-ME/SDS washes and that slight staining intensity increase is noticed with repeated washes. They later reported that 2-ME/SDS treatment before antigen retrieval generally enhances the strength of staining (Scalia et al., 2016).

2.3 Virtual microscopy

Whole slide imaging is the automatic scanning of the entire sample with an appropriate microscope, illumination system, slide mover and focusing system to produce a digital copy of the sample (Ghaznavi et al., 2013). The system automatically detects the sample on the slide and only scans the sample area disregarding the rest of the slide (Higgins, 2015). Sample depth can vary within the slide, and the system creates a focal map of the Z-depth of the sample so that an in-focus image is acquired (Higgins, 2015). The virtual microscope image is assembled from individual photographs taken from the sample, and the final virtual image can be viewed with appropriate software, much like viewing the sample under the microscope (Ghaznavi et al., 2013). Virtual microscopy systems come with the capability to image both light microscopy and fluorescent samples or just light microscopy samples (Rojo et al., 2006).

Having a virtual image of the entire slide is useful for fluorescent applications since fluorescent stains fade with time (Al-Janabi et al., 2012). A virtual image is also compulsory to capture in a protocol where an elution protocol erases the fluorescent signal and the sample is restained. The images generated from the sequential stainings can be aligned using the DAPI signal (Bolognesi et al., 2017; Gerdes et al., 2013).

2.4 Type 1 diabetes

2.4.1 Type 1 diabetes: disease overview

T1D is an autoimmune disease, where the insulin-producing beta cells of the Islets of Langerhans in the pancreas are destroyed (Ghazarian et al., 2013; Spagnuolo et al., 2013). This autoimmunity is likely mediated by autoreactive T cells (Knip & Simell, 2012; Pugliese et al., 2014). The resulting insulin deficiency in the blood leads to hyperglycemia and insufficient sugar intake to the cells of the body.

T1D often starts developing at a very young age. Progression from the preclinical state, where auto-antibodies against antigens in the pancreas develop, to the disease state can take from a few months to more than 20 years (Hyöty & Knip, 2014). T1D is one of the most common chronic autoimmune diseases in children, and it accounts for around 1-5% of all diabetes cases (Ghazarian et al., 2013). The treatment of T1D has progressed but is still expensive since life-long daily injections are required. T1D increases the risk of cardiovascular disease among other diseases and decreases life expectancy (DiMeglio et al., 2018).

As information about the disease pathogenesis has increased, the complexity of the underlying disease mechanisms has also become apparent (DiMeglio et al., 2018). The duration of disease onset varies a lot from case to case, and some patients never develop the disease although the preclinical symptoms arise (Ghazarian et al., 2013). T1D is getting more common in the Western world although the portion of diagnosed cases with the HLA risk genotype has decreased (Gillespie et al., 2004; Hermann et al., 2003). Both genetic and environmental factors contribute to the disease. Although the environmental risk factors for T1D have not been distinguished, they do play a role, since the rapid increase in T1D onset is not explained by genetics (Åkerblom et al., 2002).

2.4.2 Environmental causative factors

Many environmental factors have been studied for their contribution to T1D. The recently ended large-scale TRIGR intervention study on baby milk formula's effects on T1D concluded that hydrolyzed milk formula without complex dietary proteins did not decrease the incidence of T1D when compared to regular milk formula in high-risk patients (Writing Group for the TRIGR Study Group et al., 2018). The BABYDIET intervention study concluded that late gluten exposure did not decrease the incidence of T1D when compared to a control group (Beyerlein et al., 2014). Vitamin D deficiency, toxins and decreased gut microbiome diversity have also been studied in their relation

to T1D, and a pilot trial for vitamin D deficiency in relation to T1D has been started (Baidal et al., 2018).

EVs and T1D have been associated in many studies. Initially, T1D and EVs were associated in humans by the seasonal pattern of disease onset that followed the seasonality of EV infections (Gamble & Taylor, 1969). An elevated EV antibody concentration in T1D patients compared to controls was also measured (Gamble et al., 1969). In tissue studies, EVs have been found in the majority of pancreases of T1D patients (Hyöty & Knip, 2014). A meta-analysis reviewing the connection between EVs and T1D from 33 studies conducted between 1990 and 2010 found a significant association between EV infection and T1D and T1D autoimmunity (Yeung et al., 2011). More recently the large prospective Finnish Type 1 Diabetes Prediction and Prevention (DIPP) study has shown a time-dependent association between EV infection and the onset of T1D (Hyöty, 2016). Another large prospective study The Environmental Determinants of Diabetes in the Young (TEDDY) is also assessing the association between EVs and T1D (TEDDY Study Group, 2007). Prospective studies cannot tell whether the association is causal. Therefore, an intervention study, such as treatment with antiviral drugs or a vaccine targeted against selected enterovirus types helps to prove causality.

Since T1D is considered as an autoimmune disease, immunosuppressive drugs have been tried in intervention trials to prevent T1D. The trials have failed, which has undermined the importance of the immune system's function in the progression of the disease. This puts even more weight on environmental factors as causative agents. (Hyöty & Knip, 2014)

2.4.3 Enteroviruses

EVs and more specifically coxsackieviruses have been associated as triggering factors leading to T1D onset (Hyöty, 2016). EVs are small positive single-stranded non-enveloped RNA viruses with an icosahedral capsid surrounding the RNA genome (Fig. 4) (Harris & Coyne, 2013). EVs are the most common human viruses with more than 100 different serotypes (Knip & Simell, 2012) causing numerous diseases, although most enteroviral infections are symptomless (Hyöty & Knip, 2014). Polioviruses cause poliomyelitis; rhinoviruses cause the common cold while coxsackie A viruses (CV-A) have been linked to hand foot and mouth disease (Mao et al., 2014). Coxsackie B viruses (CV-B), on the other hand, can cause acute myocarditis (Blauwet & Cooper, 2010) and meningitis (Robinson et al., 2014). CV-B1 has been identified as a T1D risk virus in the DIPP study (O. H. Laitinen et al., 2014; S. Oikarinen et al., 2014).

Enteroviruses enter the body via the gastrointestinal tract. The viruses replicate in the epithelial cells of the mucosa and the lymphatic tissue of the gastrointestinal tract and oropharynx (M. Oikarinen et al., 2012; Rhoades et al., 2011). The viruses then enter the bloodstream via lymphatic tissue (Racaniello, 2006).

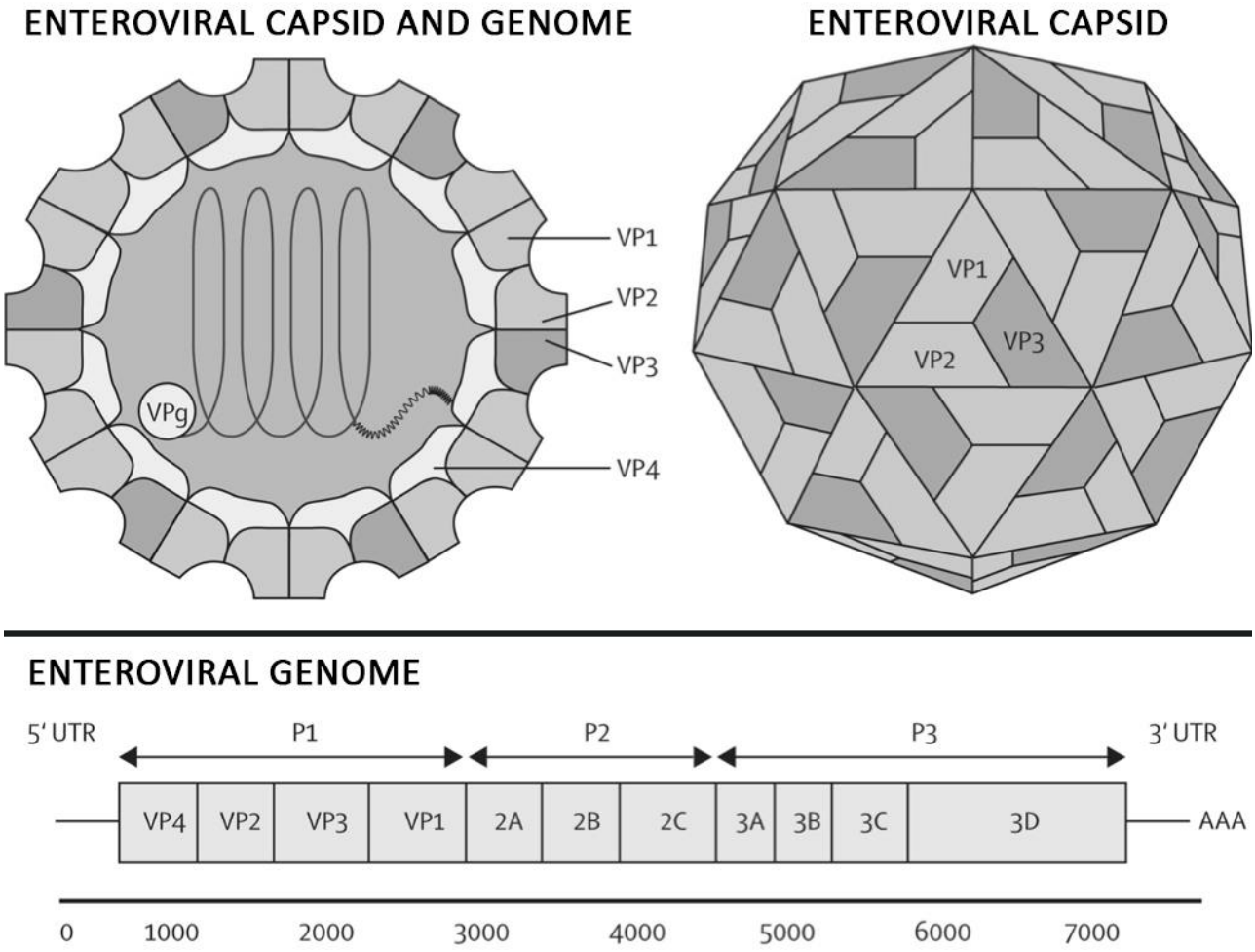

Figure 4. A representation of the enteroviral capsid and genome. Four viral proteins VP1, VP2, VP3, and VP4 form the viral capsid, with VP1, VP2, and VP3 facing outwards. Inside the capsid, the genome is shown with a genome-linked viral protein (VPg) attached. Below the enteroviral genome is represented in full length with the three genomic regions P1, P2, and P3. P1 codes for the structural proteins whereas P2 and P3 code for non-structural proteins. The genome is flanked by 5' and 3' untranslated regions (UTRs). Image adapted from Solomon et al. (Solomon et al., 2010).

2.4.4 Tissue samples and nPOD

Studying T1D pancreases *in situ* has been difficult due to the problematic location of the organ and limited accessibility for biopsies (Chapman et al., 2012). Two large research projects the Network for Pancreatic Organ donors with Diabetes (nPOD) and the Persistent Virus Infection in Diabetes Network (PEVNET) have been set up to collect tissue material from T1D organ donors for better access to tissue samples (Hyöty & Knip, 2014). Also, the Diabetes Virus Detection study (DiViD) collecting pancreatic tissue samples from recently diagnosed type 1 diabetics was conducted recently (Krogvold et al., 2014). The participants in were alive and had a part of the pancreas surgically removed in this small scale trial study. Due to unexpected complications, the study was not continued.

nPOD collects tissues posthumously from T1D patients, auto-antibody positive patients (AAb+) and non-diabetic controls. The tissues collected in addition to pancreas include pancreatic lymph node (PLN), spleen, thymus, duodenum, and blood (Pugliese et al., 2014). nPOD tissue samples are distributed to T1D researchers, and the data gathered from the research is shared in real time with other research groups working on the same topic i.e., T1D and EVs. Data sharing is logical since researchers work on tissue samples from the same patients.

nPOD tissue collection offers a unique opportunity to study the presence of EVs in relation to T1D. The pancreas is the most studied organ when it comes to T1D virus studies, and it has already been shown that EVs can be more frequently found in the pancreas of T1D patients than controls. More specifically the EVs are found in the insulin producing beta-cells in the pancreatic islets of Langerhans (Fig. 5) (M. Oikarinen et al., 2018; Richardson et al., 2009). The intestine of T1D patients is also more frequently EV-positive compared to control patients (M. Oikarinen et al., 2018, 2012). To date, the spleen of T1D patients has not been widely studied for EVs. According to one recent publication, however, the EV VP1 positivity was also found to be more prevalent in T1D patients' and AAb+ patients' spleens than in spleens of controls' (M. Oikarinen et al., 2018), making the spleen an organ of interest for further studies.

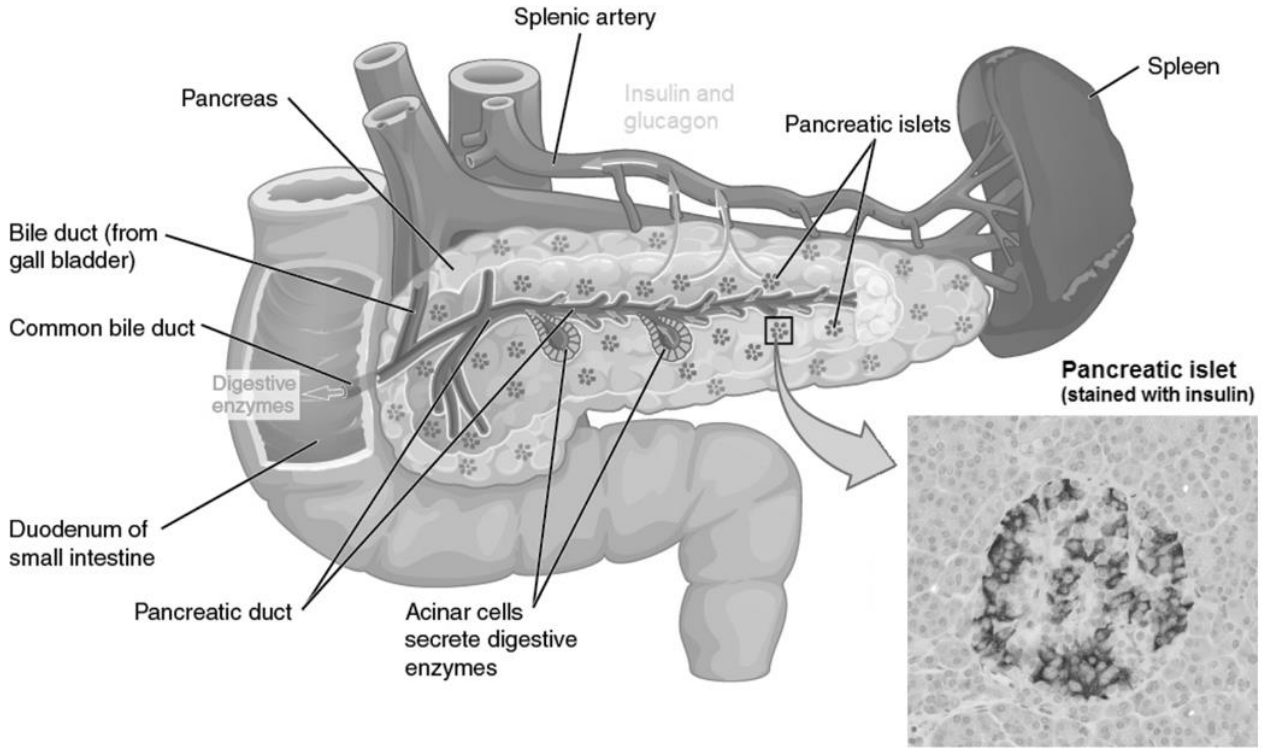

Figure 5. The anatomy of the pancreas, duodenum and the spleen. The pancreas secretes digestive enzymes to the duodenum and is right next to the spleen. A close-up of a pancreatic islet of Langerhans is shown with insulin staining. The insulin-secreting Beta-cells stained for are also often found to be VP1 positive. Image adapted from OpenStax Anatomy and Physiology textbook (http://philschatz.com/anatomy-book/contents/m46685.html 13.09.2018).

2.5 Spleen

2.5.1 Spleen morphology and function

The spleen is an organ located in the upper left abdomen and is in contact with the stomach and the pancreas (Fig. 5) (Mebius & Kraal, 2005). The spleen is a secondary lymphatic organ, which filters microbes and old erythrocytes from the blood. It is a fundamental site for lymphocyte recirculation, but it also functions as a storage for B cells, platelets and likely for monocytes as well (Steiniger, 2015).

The spleen can be distinguished into separate compartments. The red pulp is where blood is filtered with a unique open vasculature system present only in the spleen (Fig. 6). Blood in the red pulp moves in cords made of reticular fibres and fibroblasts but lacking endothelial cells. The blood is filtered by red pulp macrophages abundantly present in the cords, and the blood reenters circulation via venous sinuses, which gather the blood back into veins. (Mebius & Kraal, 2005)

The white pulp is a concentration of lymphocytes present around the splenic arteries embedded in the red pulp (Steiniger, 2015). The white pulp can be further divided into the

perilymphatic region (PALS) where T cells are concentrated and follicles where B cells are concentrated (Fig. 6) (Steiniger, 2015). The lymphocytes arrive in the spleen via open circulation and are attracted to the outside of the arteries forming the white pulp (Steiniger, 2015). The T cells making up the PALS interact with dendritic cells and B cells (Mebius & Kraal, 2005). In the follicles, clonal expansion of activated B cells takes place (Mebius & Kraal, 2005) within the germinal center of the follicle (Victora & Nussenzweig, 2012).

The majority of studies focusing on the histology of the spleen have been done in mice or rats. The human and rodent spleens differ in anatomy. The rat and mouse have a clear B cell compartment surrounding the PALS and the follicles called the marginal zone. In humans, this marginal zone area can be divided into an inner B cell mantle zone, that surrounds the germinal center and an outer $CD27^+$ superficial zone. In addition, mice and rats are missing the sheathed capillary structure found in humans. The sheath of these capillaries is made of B cells, macrophages and stromal sheath cells that are $CD271^+$. The sheathed capillaries are located before the capillary opens up to the open capillary structure of the red pulp. (Steiniger, 2015)

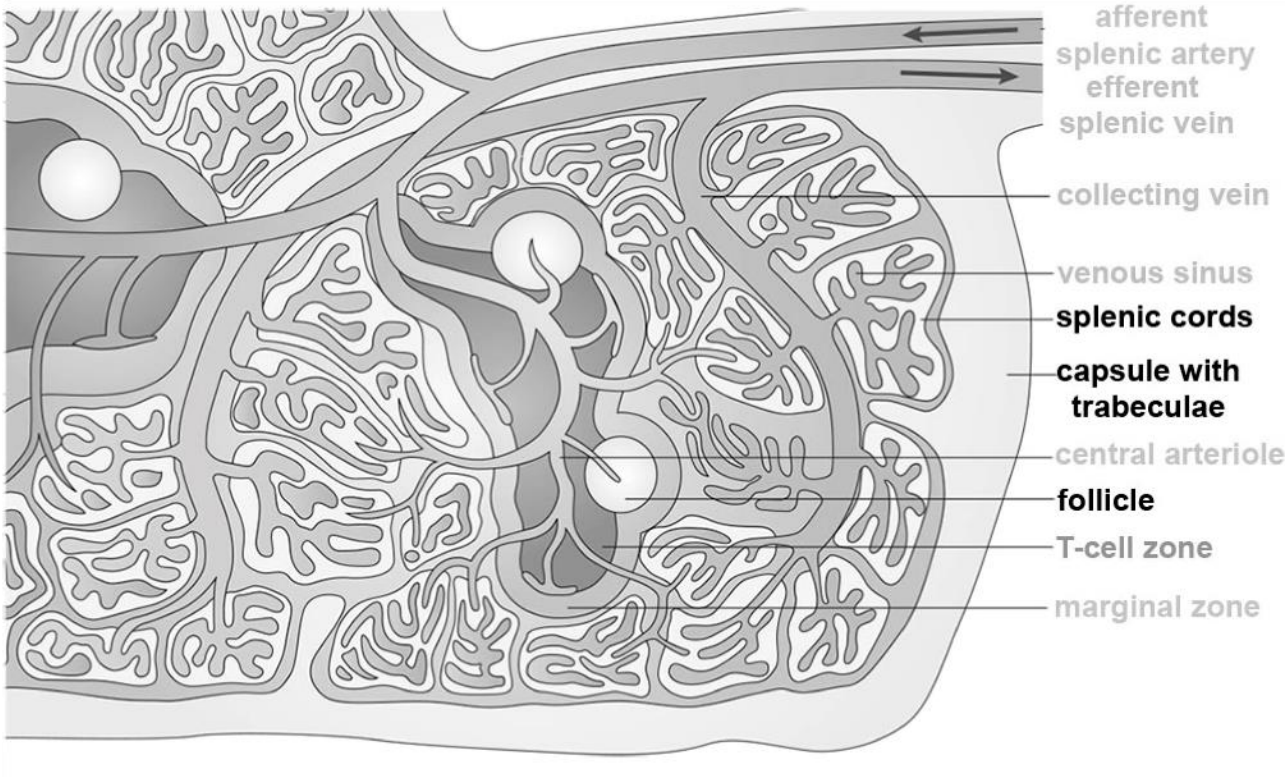

Figure 6. An illustration of the anatomy of the spleen. The illustration shows the marginal zone around the follicle and the T cell positive PALS that is found in mice. In humans, the marginal zone is further divided into an inner B cell mantle zone, that surrounds the germinal center and an outer $CD27^+$ superficial zone. Image adapted from Mebius & Kraal (Mebius & Kraal, 2005).

2.5.2 Spleen lymphocyte markers

The spleen is home to many lymphatic cell populations. PALS is made of $CD4^+$ and $CD8^+$ T cells, and it can be visualized with the common T cell marker CD3 (Steiniger, 2015). $CD4^+$ T cells are also found in the follicles (Steiniger, 2015). The PALS is primarily made of $CD4^+$ T cells with fewer $CD8^+$ T cells present (Wilkins & Wright, 2000). T cell subpopulation studies in the spleen are lacking (Steiniger, 2015). B cell subsets form the follicle and follicular surface (Steiniger, 2015). Follicular B cells are $CD20^+$, and the follicular surface B cells are $CD27^+$ (Steiniger, 2015). CD27 has traditionally been interpreted as a memory B cell marker, although $CD27^-$ memory cells are known to exist (Steiniger, 2015). The inner follicle often consists of a germinal center, where B cells proliferate (Steiniger et al., 2018). The germinal center can be divided into a dark and a light zone with a hematoxylin and eosin staining (Natkunam, 2007). The dark zone is where B cells proliferate whereas as the antigen can be found in the light zone follicular dendritic cells (Victora & Nussenzweig, 2012). In addition to hematoxylin and eosin staining, the two compartments can be distinguished with CXCR4 and CD83 or CD86. The dark zones are $CRCR4^+$, $CD83^-$, $CD86^-$ whereas the light zones are $CRCR4^-$, $CD83^+$, $CD86^+$ (Victora & Nussenzweig, 2012).

The morphology of the splenic white pulp can be further visualized with the CD271 marker that stains for fibroblastic reticulum cells and follicular dendritic cells. The fibroblastic reticulum cells make up the connective tissue in PALS whereas follicular dendritic cells support the follicle. (Steiniger et al., 2018)

Macrophages can be stained with the CD68 marker (Chistiakov et al., 2017) and the CD163 marker (Etzerodt & Moestrup, 2013). Macrophages are present in the red pulp, around the capillary sheats and in follicles (Steiniger, 2015). Since the spleen has been mostly studied in rodents, the subsets are not well defined in the human spleen, but distinctions can be made with CD68 and CD163 -markers (Steiniger et al., 2014). Red pulp macrophages stain for CD68 and CD163, whereas capillary sheath associated macrophages and follicular macrophages only stain for CD68 (Steiniger et al., 2014).

Dendritic cells are professional antigen-presenting cells activating T cells (Boltjes & van Wijk, 2014). Plasmacytoid and myeloid dendritic cells are present in the surface of the splenic follicle and the human spleen possibly contains subsets of undefined dendritic cells (Steiniger, 2015). Staining for dendritic cells is difficult since dendritic cells are difficult to distinguish from monocytes with myeloid dendritic cells and monocytes both expressing CD11c (Collin et al., 2013) and also

myeloid dendritic cell marker CD141 overlaps with the splenic sinus endothelia (Steiniger, 2015). Mature circulating dendritic cells can be stained with the CD83 marker (Breloer & Fleischer, 2008).

3 Aims of the study

The objective of this study was to set up an antibody elution workflow to permit the staining of type 1 diabetic, type 1 diabetes –related autoantibody-positive and control donor spleen samples with multiple fluorescent markers. These consecutively stained spleen samples could then be analyzed for splenic lymphocyte marker colocalization with the VP1 anti-enteroviral antibody. Multiple staining and imaging strategies were tested for the elution workflow. The study was divided into three specific aims:

1. Setting up the elution workflow for the removal of tissue-bound antibody.
2. Attaining whole slide images of subsequently stained spleen samples with the virtual whole slide scanner system.
3. Analyzing the cell types of enterovirus VP1 positive cells in the spleens of type 1 diabetic and non-diabetic controls.

4 Materials and methods

4.1 Tissue and cell samples

The samples used in this study were formalin fixed paraffin embedded (FFPE) human spleen tissue samples. FFPE coxsackievirus B1 (CB-V1) -infected and non-infected adenocarcinomic human alveolar basal epithelial cell (A549) culture samples served as positive and negative controls for enterovirus VP1. The spleen samples used were from two sources. The samples used to set up the experimental method were from the Finnish PanFin network (Tauriainen et al., 2010) and the samples used in the final experimental design were from nPOD tissue bank (Pugliese et al., 2014). The spleen samples from the PanFin network were of non-diabetic controls and will henceforth be referred to as test spleens. The test spleen samples and the cell line samples were cut to 5 µm-thick sections with a microtome and mounted on Superfrost® Plus microscopy slides (Thermo Scientific). The samples from nPOD donors were from T1D patients (N=4), AAb+ donors (N=1) and non-diabetic controls (N=4) and were cut ready to 5 µm-thick sections mounted on Superfrost® Plus microscopy slides (Thermo Scientific). The nPOD samples were recoded and randomized to not to influence the EV VP1 analysis.

4.2 Antibodies

Antibodies against the splenic lymphocytes, the splenic structural cells, and the EV were optimized by testing varying concentrations and staining conditions. The primary antibodies used in the study were all either mouse anti-human antibodies or rabbit anti-human antibodies, see Table 1. The secondary antibodies used were goat anti-mouse IgG (H+L) Alexa Fluor 488 (Life Technologies) and goat anti-rabbit IgG (H+L) Alexa Fluor 568 (Life Technologies). The Fab-fragment used was goat anti-mouse IgG (H+L) (Jackson Immunoresearch). The secondary antibodies for Fab-fragment stainings were donkey anti-goat Alexa Fluor 555 and donkey anti-mouse Alexa Fluor 488 (Life Technologies).

Table 1. Primary antibodies tested for in the study. Not all antibodies were used in the final staining of the nPOD spleen samples.

Primary antibody/antigen	Species	Clone	Dilutions tested	Source
EV VP1 protein	Mouse	5D8/1	1/100, 1/500, 1/1000, 1/1500	DAKO
CD3 general T cell marker	Mouse	NCL-CD3-PS1	1/50, 1/100, 1/150	Novocastra
CD3 general T cell marker	Rabbit	SP7	1/20, 1/50, 1/200, 1/400	Novusbio
CD20cy general B cell marker	Mouse	C26	1/150, 1/250, 1/400	DAKO
CD68 macrophage marker	Mouse	PG-MI	1/20, 1/50, 1/100	DAKO
CD83 mature dendrite cell marker	Mouse	ab49324	1/25, 1/50, 1/100	Abcam
IgM receptor marker	Rabbit	Polyclonal	1/150, 1/500, 1/600	DAKO
CD4 helper T cell marker	Mouse	N1UG0	1/50, 1/100	ThermoFischer
CD271 spleen morphology marker - fibroblastic reticulum cells and follicular dendritic cells	Mouse	ME20.4	1/50, 1/100 1/500	BioLegend
CD163 macrophage marker	Mouse	NCL-CD163	1/100	Novocastra
CD177 neutrophil marker	Mouse	WH0057126M1-100UG	1/100	Sigma-Aldrich

4.3 The basic fluorescent staining protocol

The basic fluorescent staining protocol is a staining protocol used previously in the lab, and it was used as the core for fluorescent stainings (Saarinen et al., 2018). Briefly, to fix the sample to the slide, the sample slides were heated at 60 °C for 60 minutes. Deparaffinization was done with two changes of xylene (2x5 min), and rehydration was done with four washes of ethanol and water (99 % 2x2 min, 94 % 2x2 min, 70 % 1x2 min, ddH_2O 1 x 2 min). Heat-induced antigen retrieval (HIER) was performed by heating the samples in a microwave for 20 minutes at 700W with the samples immersed in a pH 6.0 citrate buffer or pH 9.0 Tris EDTA buffer. After cooling, the samples were washed in PBS (3x5 min). To reduce unspecific fluorescent background staining, the samples were stained with 0,1% Sudan black reagent (Sigma-Aldrich, St. Louis, USA) for 20 minutes and washed in PBS (3x5 min). Unspecific binding sites on the tissue were blocked using 5% normal goat serum (Vector Laboratories Inc, Burlingame, USA), followed by a wash in PBS (3x5 min). Primary antibody diluted in antibody diluent (DAKO North America, Via Real Carpinteria, USA) was pipetted on the slide. The primary antibodies were incubated in a sealed moist chamber for either 1 h at room temperature or overnight at 4°C depending on the antibody. After primary antibody incubation, the slides were washed in PBS (3x5 min) and the secondary antibody (1/300) diluted in antibody diluent was pipetted on the slide. The slides were incubated for 1 h at room temperature in a sealed moist chamber away from light. After secondary antibody incubation, all steps were done in minimal light to avoid photobleaching of the fluorescent signal. The slides were washed in PBS (2x5 min), and ddH_2O (1x5 min) and the nuclei were visualized using DAPI (Life Technologies, Eugene, USA) with incubation of 5 min. The samples were coverslipped using either ProLong Diamond antifade mounting medium with DAPI (Life Technologies, Eugene, USA) or fluorescent mounting medium (DAKO North America, Via Real Carpinteria, USA) and were left to cure. When coverslipped with Prolong Diamond antifade mounting medium, the samples were not separately stained for DAPI.

4.4 Modified fluorescent staining protocols

4.4.1 Fluorescent double staining protocols

Two double staining protocols were tested in the study: a cocktail protocol and a Fab-fragment blocking protocol. In the cocktail protocol, the basic fluorescent staining protocol described above was used, by applying an antibody cocktail of primary and secondary antibodies, respectively.

The Fab-fragment staining protocol was tested since most of the antibodies used in the study were raised in mice and could not be combined into a cocktail. In the protocol, again, the basic fluorescent protocol was used as a backbone, and the primary and secondary antibodies were applied sequentially. Both primary antibodies were applied using their optimal dilutions and incubation times, either 1 h at room temperature or overnight at 4 °C. The Fab-fragment was used as described in the Review of the literature ("Staining for multiple antibodies simultaneously using the Fab-fragment"). Briefly, after 1 h incubation of the first primary antibody, the Fab-fragment was incubated for 1 h, followed by a secondary antibody incubation. After the Fab-fragment step, the standard protocol was followed. Blocking with normal goat serum was emitted to avoid possible cross-reactivity with remnant goat-antibodies.

4.4.2 Fluorescent single staining protocol with a counterstain

The basic fluorescent single staining protocol was modified to contain a counterstain that the virtual whole slide scanning system could recognize. Initial stainings were done without a counterstain since the natural color of the test spleen samples was strong enough for the virtual microscopy system to recognize. However, the natural color of spleen sections varied from sample to sample, and nPOD spleen samples did not have enough strong color for the system to recognize.

Although the virtual whole slide scanning system had fluorescent scanning capabilities, it relied on a brightfield method for sample recognition. Chromogenically stained samples have hematoxylin as a counterstain, which with its deep blue color is easily recognized by the system. As the scanner manufacturer did not supply a protocol for counterstaining that would have been suitable for fluorescently labeled samples, a counterstaining method for such was developed.

Although hematoxylin is known to reduce fluorescent signal (Chilosi et al., 1983), it was tested as the first counterstain, since it was known to be used in the University of Tampere for fluorescent stainings when the fluorescent signal was very strong (Open communication with histology core, University of Tampere). In this study, hematoxylin (Histolab, Gothenburg, Sweden) was diluted well beyond its typical dilution to achieve a solution where it would only slightly stain the sample to preserve the fluorescent signal but still have enough strength for the scanning system to recognize the sample. The tested hematoxylin dilutions were 1/4, 1/8, 1/16, 1/32 and 1/48 (diluted in ddH_2O). The hematoxylin staining step was added to the basic fluorescent staining protocol before DAPI-staining.

In addition to hematoxylin, Sudan black (Sigma-Aldrich, St. Louis, USA) was tested as a counterstaining reagent, since Sudan black was seen to slightly stain the spleen sample blue when used in the basic immunofluorescence staining protocol but not to affect the immunofluorescence signal. A stronger dilution of Sudan black was tested for counterstaining the test spleen tissue. The tested Sudan black concentrations were 0,1%, 0,5% and 1,0%. When Sudan black was used as a counterstain, the basic immunofluorescence staining protocol remained the same, but the incubation time of Sudan black was shortened from 20 minutes to 8-10 minutes, depending on the Sudan Black concentration. The modified basic immunofluorescence protocol with a stronger 1% Sudan black dilution was used to counterstain the nPOD human spleen samples.

4.5 Antibody optimization

A set of antibodies were optimized for the spleen samples. The tested antibody concentrations (Table 1) and incubation times were decided based on manufacturer recommendations and antibody dilutions used previously in chromogenic staining. Optimization was done using the basic immunofluorescence staining protocol with test spleens for all the immune cell markers and with the CV-B1 -infected A549 cells for the VP1 antibody.

Only the primary antibody conditions were optimized. The secondary antibodies were all incubated for 1 h at room temperature with a dilution of 1/300. Antibody signal strength was evaluated by assessing the stained tissue with Olympus BX60 microscope equipped with Olympus Colorview U-CMAD2 camera and by whole slide imaging with the virtual whole slide scanning system. The optimal antigen retrieval solution, either citrate buffer pH 6.0 or Tris EDTA pH 9.0, was tested for each antibody.

4.6 Antibody elution workflow, elution protocols and elution solution preparation

4.6.1 General elution workflow

Testing of elution protocols was done on test spleen tissue samples stained with CD3, CD20, CD68, and IgM markers and on CV-B1 -infected and uninfected A549 cells stained with the VP1 marker. During all stages of the initial staining and the subsequent elution protocol, the samples were kept moist to avoid epitope masking. In one CD20 staining, the effect of tissue drying on epitope masking was tested.

Stained and mounted samples had their coverslips removed by immersing the slides in PBS -filled Coplin jar on a shaker with heating. The temperature of the PBS was approximately 40 °C, with some variation. The incubation time of the slides also varied depending on how easily the coverslip came off. Often the coverslip did not fall off the slide on its own and had to be gently removed manually. After coverslip removal, the slides were incubated in PBS to remove all mounting medium.

After coverslip removal, the basic fluorescent single staining protocol with modifications was performed. The initial staining steps up to Sudan black staining were emitted from the elution protocol, and the first step was incubating the slides in the elution solution (described in 4.6.2 and 4.6.3). Subsequent staining was performed according to the basic fluorescent single staining protocol. This rotation of staining, imaging and removing the old fluorescent stain could be repeated and the slide could be stained with multiple markers one after the other. In this study, a single sample was given a maximum of four rotations of elution with five different markers stained.

The effectiveness of the different elution solutions was tested by doing a single staining protocol and then performing the antibody elution step. The next round of staining was modified not to contain primary antibody incubation at all. The tissue was only stained with the secondary antibody appropriate for the primary antibody that the tissue had initially been stained with. This tested if the elution protocol had left the primary antibody on the tissue and only removed the secondary antibody attached to this primary antibody.

4.6.2 Glycine SDS pH2 elution protocol and elution solution preparation

The glycine SDS pH2 elution protocol was modified from Pirici et al. (Pirici et al., 2009). In the protocol described by the authors, the tissue samples reentering staining were given a minimum of 30-minute treatment in glycine SDS pH2 solution at 50 °C in a shaker. In this study, the elution solution was preheated to 50 °C in a water bath. The temperature of the elution solution decreased during incubation because the shaker was not well insulated. The elution step was tested for 30 and 60 minutes. After the elution step, the sample was thoroughly washed for 1 h in PBS-tween with changes.

The glycine SDS pH2 solution was prepared according to Gendusa et al. (Gendusa et al., 2014). 0,94 g of glycine was added to 25 ml of 20% SDS solution. The volume of the solution was

then increased to 500 ml with ddH_2O. Finally, the pH of the solution was adjusted to pH 2 with HCl in a fume hood. The solution was stored at 4 °C.

4.6.3 2-Mercaptoethanol, SDS buffer elution protocol and elution solution preparation

The 2-Mercaptoethanol, SDS buffer (2-ME/SDS) elution protocol was modified from Gendusa et al. (Gendusa et al., 2014). The authors performed the elution at 56 °C for 30 minutes in a shaker. Initial testing of the 2-ME/SDS elution solution was done in the shaker with 30 minute and 60 minute incubation times. Due to limitations with the insulation of the shaker available, the temperature of the 2-ME/SDS could not be kept at 56 °C. In another paper, the authors tested the 2-ME/SDS elution solution at 95 °C for 10 minutes without a shaker (Scalia et al., 2016). Later testing was done in a water bath without agitation for 30 minutes at 60 °C and for 10 minutes at 95 °C. After the elution step, the sample was thoroughly washed in ddH_2O for 1 h with four changes of water.

2-ME/SDS solution was prepared as previously described by Gendusa et al. (Gendusa et al., 2014). 20 ml of 10 % w/v SDS was mixed with 12,5 ml of Tris-HCl (0,5M, pH 6.8) and 67,5 ml of ddH_2O. 0,8 ml of 2-Mercaptoethanol (Merck, Darmstadt, Germany) was then added under a fume hood. The solution was stored at 4 °C, and all elution steps with 2-ME/SDS were done under a fume hood.

4.7 Virtual microscopy

The scanning of tissue samples was done with a SlideStrider virtual microscopy system (JiLab, Tampere, Finland) equipped with an Olympus BX43 microscope and Objective Imaging Surveyor software (Objective Imaging Ltd). Scanning was done using x 10 or x 20 lens using the fluorescent filter set (Semrock, 432-523-702-HC Triple-band Filter, 409-493-596-HC Triple Dichroic mirror) and brightfield microscopy. The (fluorescently) stained samples were scanned first using brightfield microscopy and then with the fluorescent DAPI-channel, followed by green and red fluorescent channels.

A set of samples was scanned either with a fixed focusing distance set at the beginning or by focusing each slide individually. The focusing of samples was done automatically by the system using brightfield microscopy. The parameters for focusing depth, focus point distance, preview map opacity threshold and preview map particle size were adjusted for from batch to batch.

The consecutive scanning of test spleen samples stained using different fluorescent markers was performed with the system. These scans were then processed into a single stacked file (per sample), where navigation between the different scanned markers was possible. An original barcode software was engineered for the elution and rescanning workflow, with which the imaging software recognized a slide that had been scanned before and could use the original contrast map of the sample to determine the scan area for subsequent scans. The barcode software and the method for stacking scanned tissue samples were built with the help of JiLab staff member Onni Ylinen.

4.8 Staining and imaging the nPOD spleen tissue samples

The nPOD spleen tissue samples were stained five times with four rounds of antibody elution. The elution step was performed with 2-ME/SDS for 30 minutes at 60 °C without agitation in a water bath under a fume hood. The first staining was for enterovirus positivity with the VP1 antibody. CV-B1 -infected and uninfected A549 cells were used as positive and a negative controls. The slides were then scanned, and the virtual microscopy scans were analyzed for VP1 positivity. The analysis was done by going through the whole section manually with JVSview software (http://jvsmicroscope.uta.fi/?q=jvsview). VP1 positivity that was weak or seemed like unspecific staining was disregarded.

The VP1 positive locations were marked on the scanned image and relocated with the virtual microscopy system on the tissue sample. The VP1 positive sites were then manually reimaged for both the green channel stained with VP1 and for the blue channel stained with DAPI using the x 40 lens. Manual reimaging gave an image that was completely in focus. The coordinates for each image were noted for later imaging.

Based on the morphology of the VP1 positive cells the order of subsequent stainings was decided. The samples were subsequently stained with CD68, CD3, CD20, and CD83 in the listed order. After each staining, the sample was imaged for the marker stained for and for DAPI. CD83 staining was only performed for selected samples (N=5), due to the small amount of antibody. After the VP1 staining, the slides were not scanned and only the previously VP1 positive locations on the sample were imaged using the x 40 lens. The sites were found with the coordinates noted in the VP1 staining, and the field of view was aligned with the VP1 positive location with the aid of the DAPI channel.

Once all samples were imaged for all markers, the images were combined with Adobe Photoshop (Adobe Systems Incorporated, San Jose, USA) by individually stacking the image taken for each marker with the VP1 positive image. Since each primary antibody used was raised in mouse, and the only secondary antibody used in the staining was Alexa Fluor goat anti-mouse IgG (H+L) 488, all positive signal was in green color. VP1 signal was kept green, but the signal of the other markers was pseudocolored using the hue settings in Adobe Photoshop. Mixing of images into a merged image with the signals of multiple stainings was done using the lighten blending mode. Combining the images was partially automated using Keyboard Maestro software (Stairways Software Pty Ltd, Nobby Beach, Australia). The exact aligning of the images was done manually by comparing the DAPI channels of each image. This was done by stacking subsequent images into layers and by decreasing one of the DAPI layers opacity in Photoshop to allow the comparison of nuclei. The layers could then be moved to align. Once images were overlayed, the colocalization of the VP1 signal with the signal of the other stainings could be analyzed.

4.9 Image analysis

The intensity and type of the VP1 signal and its colocalization with the other antibodies was analyzed and quantified in the following ways: VP1 signal intensity was quantified on a scale from one to three, where one indicated weak signal, two indicated moderate signal and three indicated strong signal. The location of the VP1 signal was determined to be either in the whole cell or only in a part of the cell. The morphology of the VP1 positive cell was determined to be either round and small, large and uneven or something else.

The colocalization of the VP1 signal with each of the subsequently stained antibodies was analyzed on a scale of zero to two, where zero indicated no colocalization, one indicated some colocalization and two indicated that the two signals mostly colocalized. The staining intensity of the colocalized CD68, CD3, CD20 or CD83 signals at the site of VP1 positivity and in the same cell as VP1 positivity was assessed on a scale of zero to three. Zero indicated that the two signals did not colocalize, one indicated that the strength of the colocalized signal at the site of VP1 positivity and in the same cell as VP1 positivity was weak. Two indicated that the colocalized signal at the site of VP1 positivity and in the same cell as VP1 positivity was moderate, and three indicated that the colocalized signal at the site of VP1-positivity and in the same cell as VP1 positivity was strong. The positivity for CD68, CD3, CD20 or CD83 in the surrounding cells of a VP1 positive cell was analyzed

as either true or false for each antibody, where a single positive cell touching the VP1 positive cell made the assessment true for that antibody.

The compartment of spleen for the VP1 positivity was also assessed based on the morphology of tissue at the VP1 positive location and the strength and prevalence of $CD3^+$, $CD20^+$ and $CD68^+$ cells in the area.

5 Results

5.1 Antibody optimization

Different incubation times and temperatures were tested to find the optimal conditions for the antibodies. Optimization was performed using spleen sections from non-diabetic donors from the PanFin network. Of the antibodies tested for immunofluorescent staining, not all were suitable. The CD4 and CD3 (clone SP7) antibodies did not produce a noticeable signal. The CD271 antibody gave too weak a signal and was disregarded. The CD163 and CD177 antibodies gave clear positive signals; however, as they were available only in small quantities they were not used for the staining of the nPOD spleen sections at this point. Besides optimizing the antibody incubation time and the concentration, two different antigen retrieval solutions, pH 6.0 citrate buffer and pH 9.0 Tris EDTA buffer, were tested. As a result, no difference was observed between the two in the outcome of the antibody signal. Therefore, subsequent assays were performed using pH 9.0 Tris EDTA buffer.

CD20, CD3 (clone NCL-CD3-PS1), CD68, IgM and VP1 antibodies had previously been optimized for fluorescent stainings in the lab (data not shown). CD83 antibody had also been optimized before, but its signal was not as strong as the signal of the other antibodies. In addition to VP1, the antibodies CD20, CD3 (clone NCL-CD3-PS1), CD68 and CD83 were applied for staining the final nPOD spleen samples (Fig. 7). The optimal concentrations of used antibodies were CD20 (1/400), CD3 (1/100), CD68 (1/100), CD83 (1/25), and VP1 (1/100). These antibodies stained a large pool of cells and could give a broad overview of how the VP1 signal colocalized.

The strongest signal for all antibodies at the lowest concentration was attained using an overnight incubation at 4 °C. This incubation step was used for all antibodies except VP1 in the nPOD spleen sample staining. VP1 antibody was applied for 1 h at room temperature. The antibodies CD20, CD3 and CD68 did not give any unspecific background signal with either 1 h room temperature or overnight 4 °C incubation. Faint unspecific binding of the VP1 antibody was noticed in blood vessel walls, but this was distinguishable from VP1 positive cells.

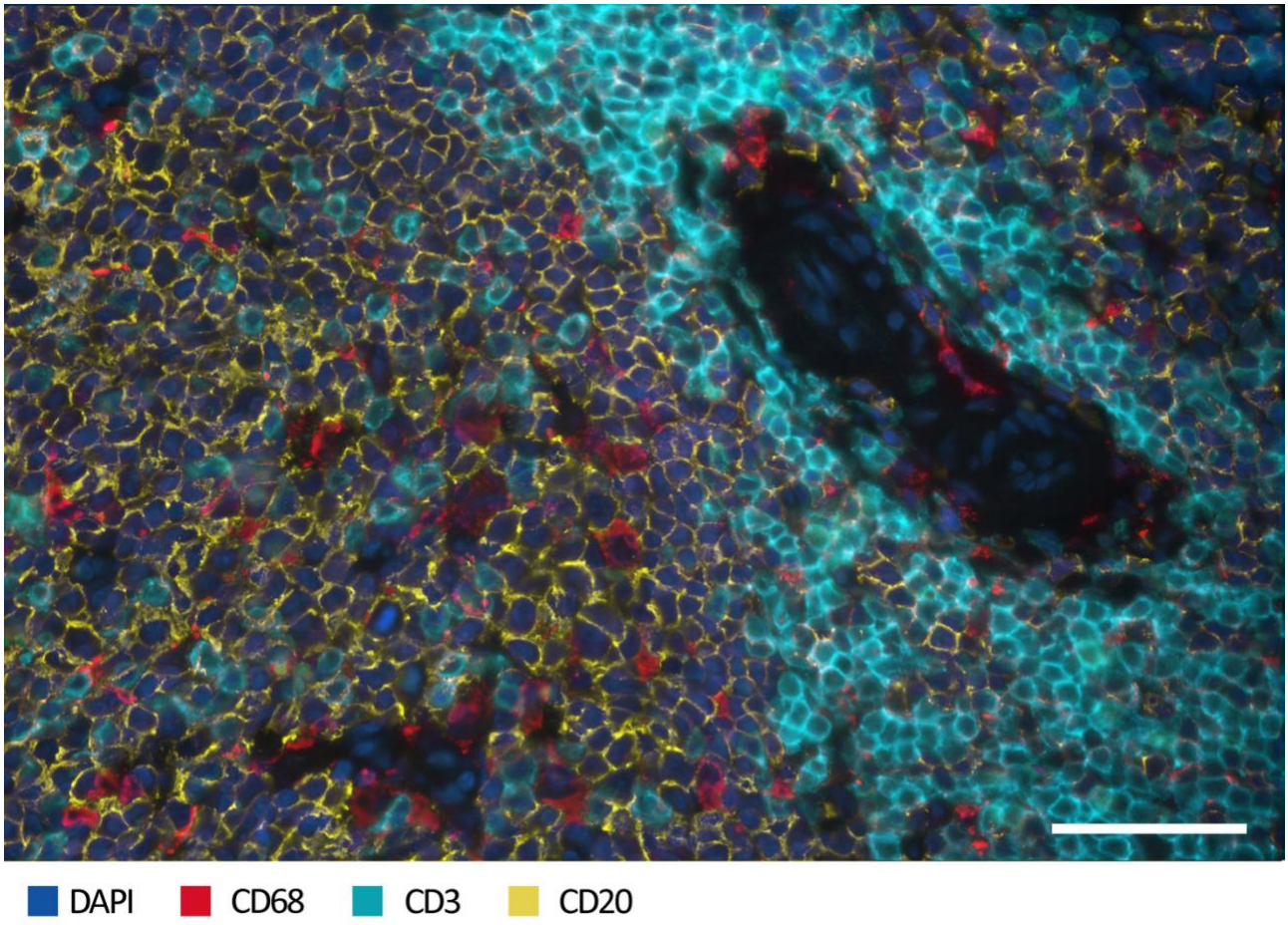

Figure 7. The human spleen stained with B cell, T cell, and macrophage markers. The $CD20^+$ B cells (yellow) make up a follicle that changes into a $CD3^+$ T cell (blue) populated PALS-region surrounding a blood vessel. $CD68^+$ macrophages (red) are also present in quite large numbers. DAPI is marked in dark blue. All signals except for DAPI are pseudocolored with Adobe Photoshop. Scale bar is 50 µm.

5.2 Fluorescent double staining protocols

5.2.1 Antibody cocktail protocol

Staining for multiple markers with a cocktail protocol is possible when antibodies from different species are available. Due to the lack of available and working rabbit anti-human antibodies, the cocktail double staining method could not be utilized for any of the final nPOD sample stainings. When testing the antibody cocktail using rabbit anti-human IgM antibody and mouse anti-human CD20 antibody, the IgM antibody was completely quenched by the CD20 antibody and did not give a signal. Staining for just IgM in the same staining round gave a strong signal (data not shown). However, the IgM marker was considered too specific for our purposes and therefore disregarded from the final stainings.

5.2.2 Fab fragment protocol

Since all the available antibodies for nPOD sample staining were mouse anti-rabbit antibodies, the Fab-fragment protocol was tested for double staining with two mouse anti-human antibodies. As a result, the Fab-fragment staining did not produce a reliable signal, with the first stained antibody showing through on the fluorescent channel of the second antibody (data not shown). The secondary antibodies used in the Fab staining did not bleed through to other fluorescent channels in other stainings. The second secondary antibody used in the Fab fragment protocol gave a strong signal for its primary antibody and a weaker signal for the first primary antibody.

5.3 Fluorescent single staining with a counterstain

Scanning of the fluorescently stained slides with the Slidestrider virtual microscopy system required counterstaining the sample for tissue recognition. Staining spleen samples with hematoxylin gave a strong counterstain, with the strength of the counterstain determined by the concentration of the hematoxylin solution. In Figure 8A, the complete scan of a test spleen tissue sample is shown with a hematoxylin counterstain. The tissue scanner recognizes a counterstain of this strength. However, staining a fluorescently labeled sample with a hematoxylin counterstain affects the strength of the fluorescent signal as seen in Figures 8C and 8E.

In contrast to hematoxylin counterstaining, counterstaining with Sudan black did not affect the strength of fluorescent signals while giving a strong enough counterstain for the tissue scanner to recognize the tissue (Fig. 8B, nPOD sample counterstained with Sudan black). The close up immunofluorescent images taken from the Sudan black counterstained nPOD spleen sample show a strong DAPI signal (Fig. 8F) and a strong CD68 signal (Fig. 8D).

The intensity of the Sudan black counterstain was significantly greater with 1,0% (Fig. 8B) at incubation times of 8-10 minutes than with a 0,1% Sudan black solution (data not shown) at an incubation time of 20 minutes. Decreasing the concentration and the incubation time of the hematoxylin solution did save more fluorescent signal, but the strength of the counterstain also decreased. Low enough concentrations of hematoxylin that preserved the fluorescent signal did not give a strong enough counterstain for the tissue scanner to recognize the tissue. Since Sudan black gave a strong counterstain without signal loss, it was used to counterstain samples scanned with the Slidestrider virtual microscopy system.

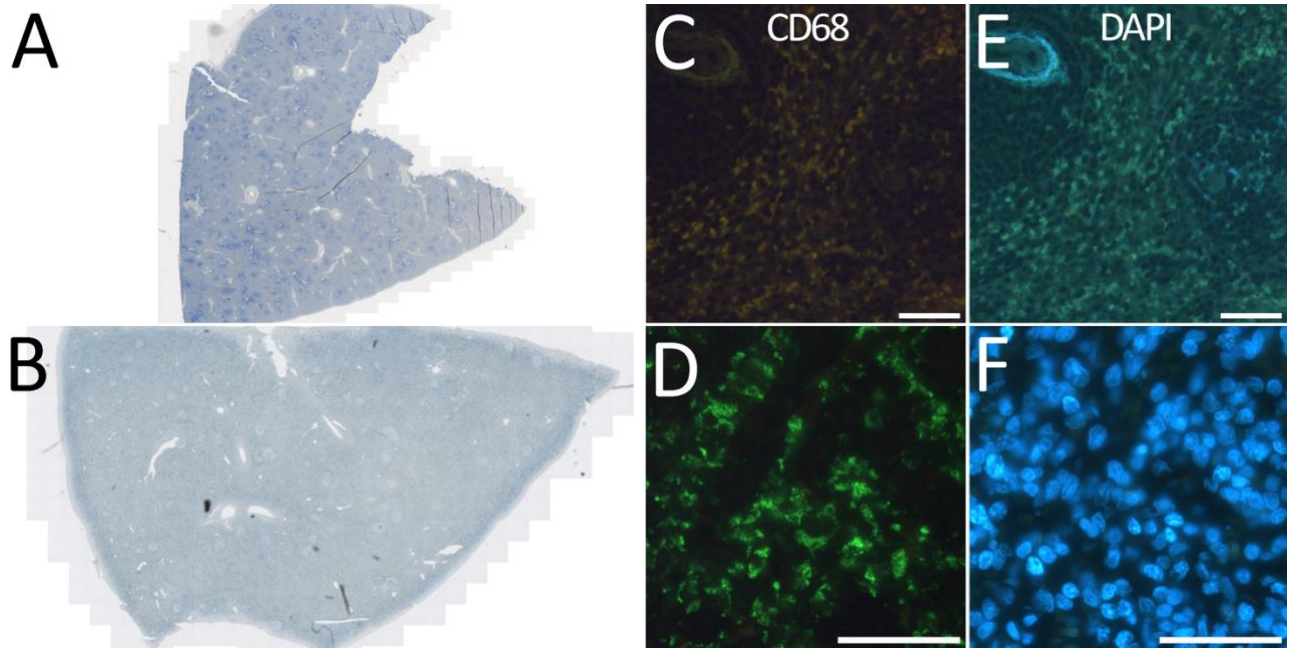

Figure 8. Comparison of counterstaining spleen tissue samples using hematoxylin and Sudan black. The results obtained with Sudan Black counterstain were superior compared to hematoxylin counterstain, as the former did not affect the fluorescent signal of the antibodies used**.** Bright field image of a scanned whole test spleen sample stained with a hematoxylin counterstain (A) and close up immunofluorescent images of CD68 (green; C) and DAPI (blue; E). Bright field image of a scanned whole nPOD spleen sample counterstained with Sudan black (B) and close up immunofluorescent images of CD68 (green; D) and DAPI (blue; F). (E) Shows how the DAPI signal of the sample is completely quenched in the staining. (C) Shows the complete quenching of the CD68 signal as well, however with some antibodies like CD20 the green fluorescent signal is not completely quenched by hematoxylin (data not shown). (C) and (E) show autofluorescent signal mostly originating from erythrocytes of the spleen. Fluorescent images of hematoxylin stained sample are obtained from a whole tissue scan scanned at x 10, whereas fluorescent images of the Sudan black stained sample are from individual locations imaged at x 40. Scale bars are 50 µm.

5.4 Elution protocol

5.4.1 General findings

A critical step in the elution workflow was the safe removal of the coverslip from the slide prior to the next staining. The binding strength of the coverslip on the slide depended on the mounting medium used, with fluorescent mounting medium binding firmly to the slide whereas ProLong Diamond antifade reagent did not bind as strongly to the slide. The binding strength also depended on the length of time between the mounting of the coverslip and the removal of it. Nonetheless, the fluorescent mounting medium was used for the final stainings.

The removal of all coverslips was accomplished by incubating them in PBS in a heated shaker. The time for the coverslip to come off varied. On some occasions, the coverslip did not fall

off in the shaker, and careful removal was done by hand. No damage to the tissue was observed after removal of the coverslip.

In the setup of the protocol, the masking of epitopes due to sample drying was tested using the CD20 marker. The intensity of the CD20 signal remained the same between a sample that was kept moist and a sample that was allowed to dry before the incubation of the primary antibody. Nevertheless, all slides were kept moist during the elution protocol.

5.4.2 SDS pH2 and 2-ME/SDS elution protocols

The removal of tissue-bound antibodies was tested with the SDS pH2 and 2-ME/SDS elution solutions. The elution of antibodies with the SDS pH2 solution gave a mixed result with some antibodies being removed from the tissue while others mostly staying bound to the antigen. In Figures 9A and 9B, the effect of SDS pH2 elution is seen on a CD68 stained spleen sample, with Figure 9B showing complete removal of the bound CD68 antibody after the elution step. In contrast, in Figures 9C and 9D the effect of SDS pH2 elution step is seen not to remove bound VP1 antibody, with Figure 9D showing nearly as strong staining for VP1 as Figure 9C.

The elution of antibodies with 2-ME/SDS solution at 60 °C removed all bound antibody for every antibody tested. There was no heated shaker available that could keep the 2-ME/SDS solution at 56 °C as described by the original publication (Gendusa et al., 2014), so no shaker was used and instead the slides were incubated at 60 °C without agitation. In Figures 9E and 9F, the effectiveness of the elution step is seen on bound VP1 antibody, with Figure 9F showing no remaining VP1 antibody bound on the sample. No change in the intensity of antibody staining was observed after multiple elutions with 2-ME/SDS. The effectiveness of 2-ME/SDS elution solution was dependent on temperature. When the 2-ME/SDS elution step was initially tested with the heated shaker where the temperature did not reach 56 °C, the elution of antibodies did not take place.

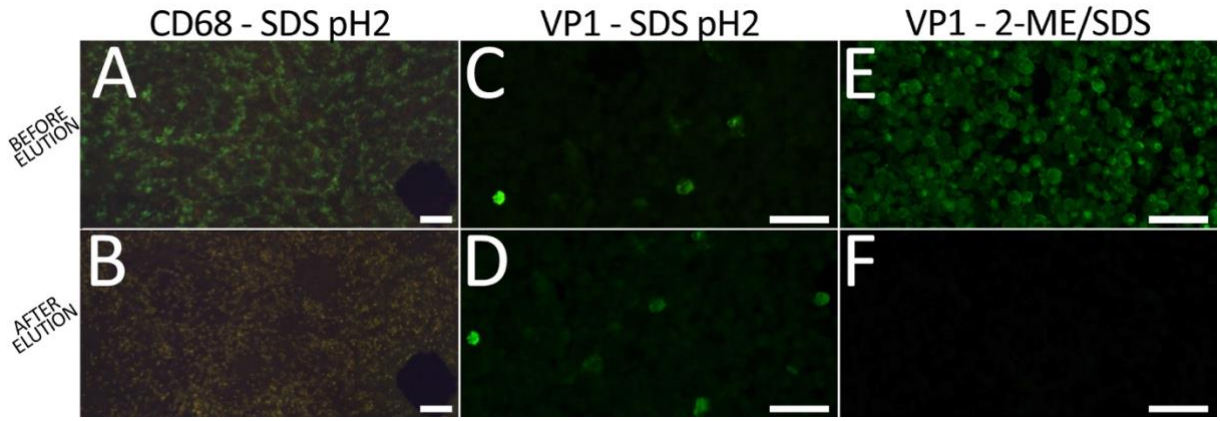

Figure 9. Elution of bound antibodies with SDS pH2 and 2-ME/SDS solutions. SDS pH2 solution was an effective elution solution for some antibodies such as CD68. (A) CD68 signal (green) on test spleen tissue. (B) After an elution step with SDS pH2, the CD68 signal is completely removed. The only signal seen is background signal of tissue, mostly originating from autofluorescent erythrocytes. (C) VP1 signal (green) on enterovirus-infected cells. (D) After an elution step with SDS pH2, the VP1 signal has only slightly weakened. (E) VP1 signal (green) on enterovirus-infected cells. (F) After an elution step done with 2-ME/SDS, the VP1 signal is not visible.

5.5 Virtual microscopy

Tissue scanning was done using the Slidestrider virtual microscopy system. The Surveyor software used by the Slidestrider did not function reliably, and the adjustment of focal place depth and focus point distance was haphazard. Often the limits given for searching the focus plane in the Z-direction were ignored by the software with the focus plane changing to a completely odd value. An example of this sort of behavior can be seen in Figure 10B, where individual tiles in the middle of the sample have a completely different focal plane from the tiles around them.

Achieving overlayed full scans was not possible when using the same saved preview map for subsequent scannings. The tissue sample scanned in Figure 10C is shown rescanned in Figure 10D using the same preview map to determine the scan area of the sample. As Figure 10D illustrates, the preview map misaligns with the tissue.

Even with a strong tissue counterstain, the formation of the preview map used by the scanner to determine the area for scanning was challenging and varied from scanning to scanning. In 10A an incomplete preview map of the tissue resulted in a scan that left out tiles in the middle of the tissue. Due to difficulties in preview map formation and other unknown problems, slides were often left unscanned by the system.

As the analysis was done on a single cell level, the quality of scanning was not good enough at x 20 magnification. However, scanning with the x 40 magnification was impossible due

to technical reasons found in the scanner. Due to many technical challenges, the nPOD samples were only scanned after the initial VP1 staining. These tissue scans were analyzed for VP1 positivity with the JVSview software, and positive locations on the tissue were reimaged manually with x 40 magnification.

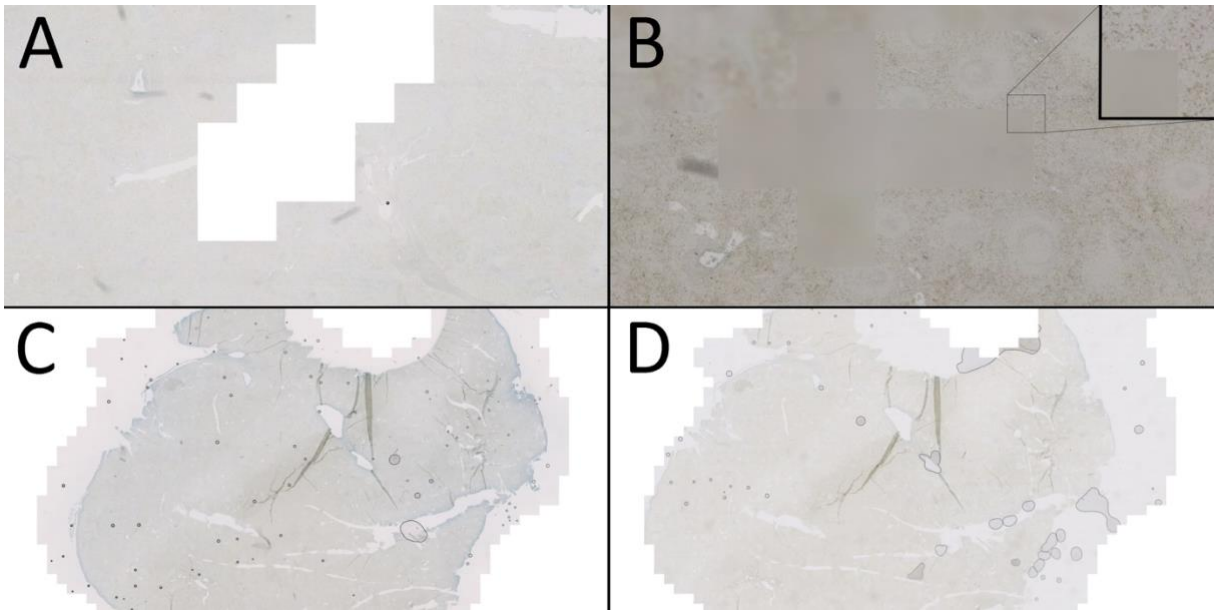

Figure 10. Problems with the scanning apparatus. (A) A scan where part of the tissue is missing in the middle of the sample. (B) Part of the tissue has been scanned at a different focal plane from the surrounding tissue leading to an out of focus scan. Smaller box showing zooming in of the border between tiles in focus and tiles out of focus. (C) The initial scan of a test spleen sample. The preview map image of the sample has been created based on this first scan and can be seen as the edge between the scanned area and the white surroundings. (D) The same test spleen sample rescanned using the same preview map. Due to inaccurate aligning of the slide between scans on the microscope table, the preview map misaligns with the tissue.

5.6 nPOD spleen tissue samples

5.6.1 General

The multiple elution steps performed on the nPOD spleen samples did not damage the tissue. Each antibody showed a similar signal when compared to previously unstained samples. The spleen contains vast amounts of erythrocytes that show autofluorescence, but this was also clearly distinguishable from the correct fluorescent signal.

5.6.2 VP1-positivity

Nine nPOD donor spleens (4 T1D, 1 AAb+, 4 control) were stained for EV VP1. As a result, strong VP1 positivity was found in individual cells. The amount of VP1 positive cells was limited, and one sample lacked strongly VP1 positive cells altogether (Table 2). No statistical evaluation of VP1 positivity could be performed due to the low number of donors per group. The VP1 positivity was punctual and followed the outlines of individual cells. The morphology of the positive cells varied. Cells were found to have either a small round phenotype (Fig. 13 merged image B) or an uneven larger phenotype (Fig. 13 merged images A and C). In addition, there was positivity that did not fit either criterion (Fig. 13 merged image D). The cells often looked only partly positive for VP1. The number of VP1 positive cells by morphology is presented in Figure 11A. Only clearly positive cells were taken into account. Cells that were only partially positive or displayed only faint positivity were disregarded. The number of VP1 positive cells in the different regions of the spleen are presented in Figure 11B.

Table 2. The nPOD spleen samples with the donor type and the number of VP1 positive cells listed.

nPOD spleen sample	Sample type (diabetic, auto antibody positive, control)	Number of VP1 positive cells
6179-01	control	11
6182-01	control	2
6195-01	T1D	2
6208-01	T1D	1
6084-04	T1D	1
6156-02	AAb+	0
6130-01	control	1
6089-02	T1D	1
6106-01	control	2

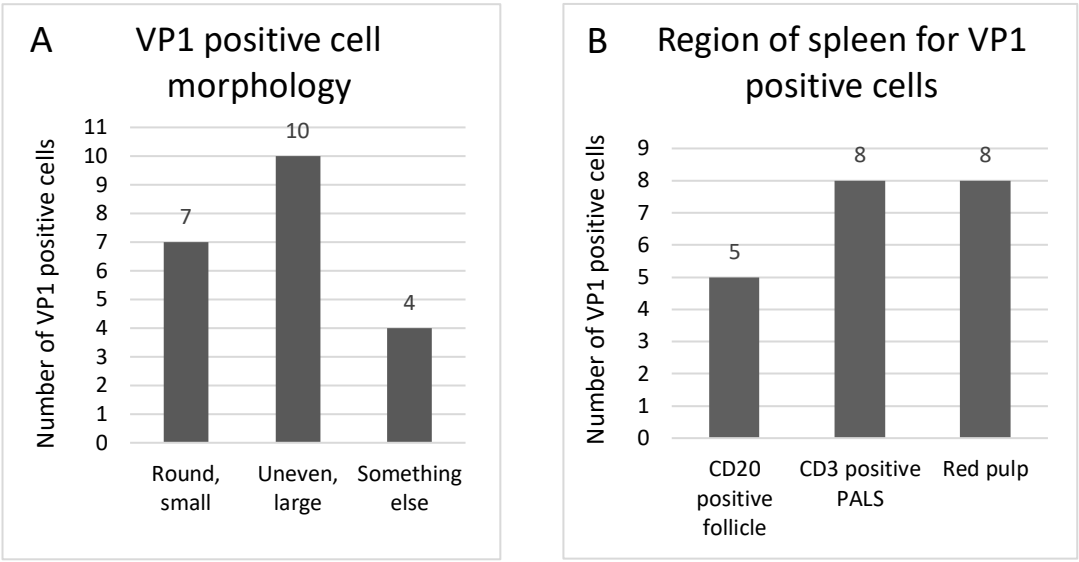

Figure 11. (A) The number of VP1 positive cells by morphology. The VP1 positive cells were categorized as follows: round and small, uneven and large and as something else. The majority were either uneven and large or round and small. **(B) The number of VP1 positive cells in different regions of the spleen.** Regions are categorized according to CD20, CD3 and CD68 positivity. $CD20^+$ follicles contain an abundance of $CD20^+$ cells, $CD3^+$ PALS contain an abundance of $CD3^+$ cells and the red pulp has a significantly lower number of CD20 and CD3 cells and is more abundant in $CD68^+$ cells. VP1 positive cells were found relatively evenly distributed across the different regions of the spleen.

5.6.3 Colocalization of other fluorescent signals with VP1-positivity

The nPOD spleen samples were stained for CD3, CD20, CD68, and CD83. Most of the 21 VP1 positive cells showed some colocalization with these markers. Only two cells did not colocalize with any of the markers studied (Fig. 12). VP1 colocalized mostly with CD3 and CD68, whereas CD20 signal showed less colocalization. This is in line with VP1 positive cells being slightly more abundant in the $CD3^+$ PALS region when compared to the $CD20^+$ follicles (Fig. 11B). The colocalization of the signals was found to be either partial or complete, and this was used as a parameter to classify colocalization (Fig. 12). In VP1 positive cells, the signal of the colocalizing marker was often found to be slightly less intense than in the surrounding cells.

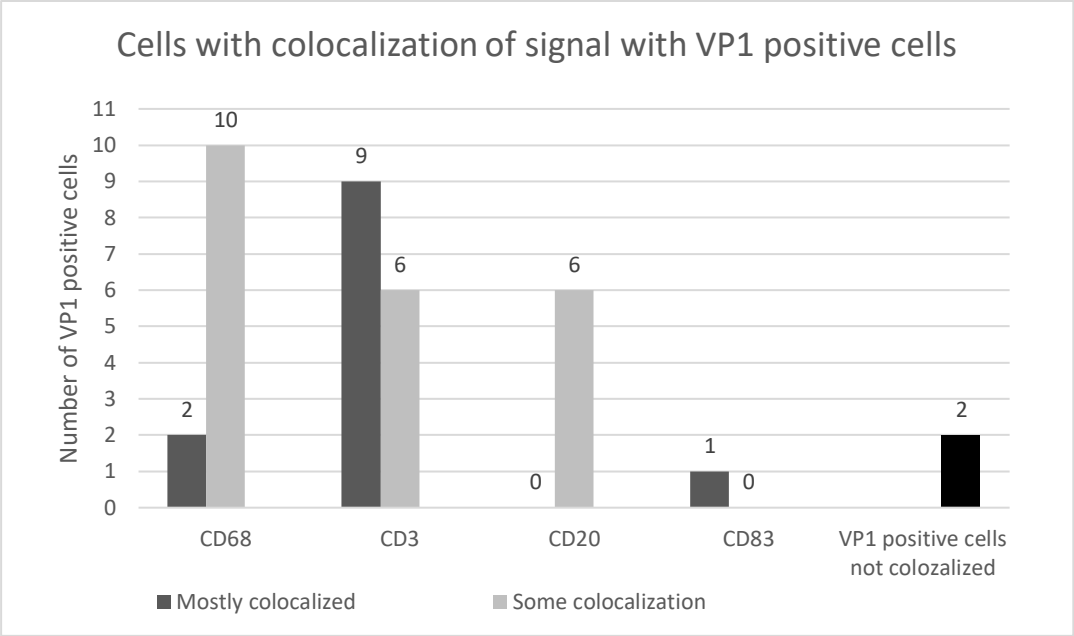

Figure 12. The number of VP1 positive cells colocalizing with CD68, CD3, CD20, and CD83. Colocalization of signals was divided into two categories: mostly colocalized and cells with some signal colocalization. Mostly colocalized cells had colocalization of most of the VP1 positive area with another marker. Cells with some colocalization were cells where only part of the VP1 positive area overlapped with another marker. VP1 positive cells that did not colocalize with any of the markers stained for are also shown. Only one cell was positive for VP1 and CD83, however, this marker was only stained for in five of nine the spleen samples. There were also several weakly stained $CD83^+$ cells that colocalized with VP1, but they were disregarded due to the weak signal.

5.6.4 Location of VP1 positivity within the spleen

The VP1 positive cells were quite evenly distributed to different regions of the spleen (Fig. 11B). VP1 positive cells were mostly found within the $CD3^+$ PALS (Fig. 13C) and red pulp (Fig. 13B), but also within $CD20^+$ follicles (Fig. 13A). Some VP1 positive cells were situated right next to blood vessels (Fig. 13D). These were categorized as part of the red pulp since no $CD20^+$ follicle nor $CD3^+$ PALS was present around the blood vessel. Faint VP1 signal was also seen inside blood vessels. This staining was diffuse and did not take the shape of a cell.

VP1 positivity was found inside a $CD68^+$ cell within $CD20^+$ follicle, partly colocalizing with both markers (Fig. 13A merged image). VP1 positive cells were also found nearby $CD68^+$ cells in the red pulp (Fig. 13B). In the PALS, the VP1 positive cells colocalized partly with CD3 (Fig. 13C merged image). Figure 13D merged image shows two VP1 positive locations in the red pulp next to a blood vessel. Both VP1 positive locations colocalize with CD3 signal fully and partially with CD68.

The staining intensity for both CD3 and CD68 -signals colocalizing with the VP1 positive locations are quite weak and cannot be seen in the merged image from underneath the green VP1 signal.

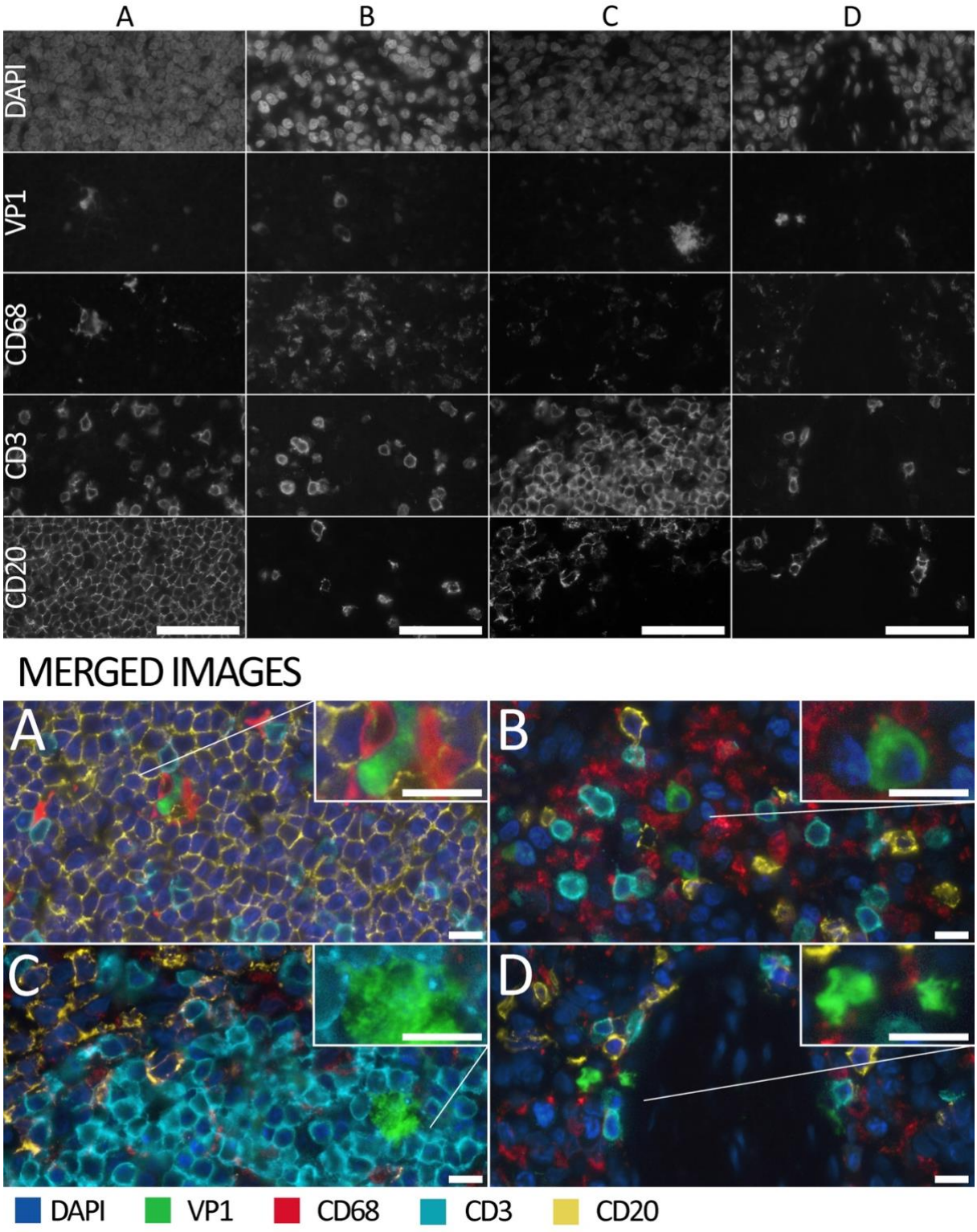

Figure 13. The colocalization of VP1 signal with CD68, CD3 and CD20 signals. Top: Grayscale images of each fluorescent stain are combined to make merged color images. Left side titles indicate the staining done for each row. The letters indicate the column making up the corresponding merged image. Bottom: fluorescent images are merged and CD68, CD3 and CD20 signals are pseudocolored. In the merged images the DAPI signal intensity has been decreased to show the other fluorescent signals better. Box shows zooming in of the VP1 positive location. (A) In the merged image a VP1 positive cell is seen inside the $CD20^+$ follicle. Although the VP1 signal is clearly inside the $CD68^+$ cell, the colocalization is graded as partial since only part of the VP1 positive area is on top of the CD68 and CD20 signals. (B) In the merged image a VP1 positive cell is seen inside the red pulp. The red pulp has fewer $CD3^+$ and $CD20^+$ cells and is more abundant in $CD68^+$ cells. Partial colocalization is seen with the CD68 signal. (C) In the merged image a VP1 positive cell is seen within the $CD3^+$ PALS with the $CD3^+$ PALS changing into $CD20^+$ follicle. (D) In the merged image, two VP1 positive locations are seen in the wall of a blood vessel. The VP1 signal colocalizes mostly with CD3 and partially with CD68. Both colocalizing signals are faint. In (A) CD20 and (C) CD3 grayscale images a dark spot is seen that do not contain much signal and align with the VP1 positive cell in the merged images. Scale bars for grayscale images are 50 µm and scale bars for merged images are 10 µm.

6 Discussion

6.1 Antibodies

Several antibodies staining lymphocytes and the structural cells of the spleen were tested. These antibodies included the lymphocyte markers CD20 (B cells), CD3 (T cells), CD68 (macrophages), CD83 (mature dendritic cells), IgM (IgM-receptor), CD4 (Helper T cell), CD163 (macrophages), and CD177 (neutrophils). In addition, the spleen structural marker CD271 (fibroblastic reticulum cells and follicular dendritic cells) was tested. The antibodies chosen for the staining of nPOD samples were VP1, CD68, CD20, CD3, and CD83. CD3, CD20 and CD68 markers reveal the morphology of the spleen. $CD3^+$ cells indicate the T cell prevalent PALS-area of the spleen, $CD20^+$ cells indicate the B cell prevalent follicle and the lower amount of $CD20^+$ and $CD3^+$ cells in addition to more abundant $CD68^+$ indicates the red pulp of the spleen.

One of the tasks of this study was to set up a protocol for staining multiple markers simultaneously. The preferred method was to stain the tissue samples using an antibody cocktail since it was the least labor-intensive method, and it is also well documented. With most of the available in-house antibodies being mouse anti-human antibodies, the design of antibody cocktails leads to the searching of rabbit anti-human antibodies. Unfortunately, most rabbit anti-human antibodies against markers of interest in this study, such as CD4, were either expensive or scarce.

The CD4 and CD3 (clone SP7) antibodies did not function in the immunofluorescent staining of the spleen although according to the manufacturer the antibodies are suitable for immunofluorescent staining and the spleen is abundant in lymphocytes expressing these antigens. Different concentrations and different unmasking solutions were tested, but this did not yield a better result. CD271 only functioned when stained chromogenically, which lead to abandoning the use of this antibody. Since chromogenically stained antibodies leave a covalently binding residue on the sample, they cannot be washed off the sample, which was not suitable for the purpose of this study.

Cocktail staining was tested with IgM since it was the only available rabbit anti-human antibody initially available. Although the antibody worked well in single stainings, it failed to function in cocktail stainings with CD20. The IgM antibody was considered too specific a marker at this stage of the study and was discarded. Even though the IgM antibody was left out of the final staining plan, experimenting with it gave valuable information about the possible difficulties facing antibody cocktail optimization.

Out of the antibodies chosen for staining the nPOD samples, CD3 was the only antibody that could be attained with an anti-human rabbit clone (clone SP7). Had the CD3 (clone SP7) antibody successfully stained spleen, it could have facilitated the use of an antibody cocktail method for staining the nPOD spleen samples in conjunction with one of the mouse anti-human antibodies. Even if rabbit anti-human antibodies were available for staining, the functioning of these in a cocktail would have had to be tested for each combination.

Since all the available antibodies for nPOD samples were mouse anti-human antibodies, the Fab-fragment protocol was tested for double staining. Unfortunately, this staining method produced an unreliable staining pattern with the first primary antibody showing positive when the second antibody was viewed. The secondary antibodies with fluorescent markers had been previously used in other stainings without problems, ruling out bleed through as a reason for this phenomenon. Since the Fab-fragment used was a monovalent antibody, there was no second binding site for the second primary antibody, ruling out crossreaction. The Fab-fragment is also polyclonal, meaning that it should cover all the different epitopes of the primary antibody.

A reason for this phenomenon may be that there were antigens available for binding on the first primary antibody not blocked by the Fab-fragment. This is a reasonable assumption in light of literature. According to Negoescu et al. a 1h incubation with the Fab-fragment blocked the binding sites of secondary antibodies selectively depending on the concentration of the Fab-fragment solution applied and the incubation time of the secondary antibody competing for binding sites (Negoescu et al., 1994). It can be concluded that more research on optimal concentrations and incubation times of the Fab-fragment and the second secondary antibody should have been conducted. These optimal concentrations and incubation times may vary from antibody to antibody making the consecutive staining of multiple antibodies laborious. In hindsight, pursuing staining with the Fab-fragment may not have been an optimal strategy for this study.

6.2 Setting up the elution workflow

To facilitate the staining of multiple markers on the tissue samples, an elution workflow was set up. In the elution workflow, each marker was stained for, followed by imaging of the sample and the elution of the bound antibody. After the elution step, the process could be repeated for each marker.

A suitable mounting medium was needed for a functional elution workflow. Although fluorescent mounting medium bound the coverslips tighter than Prolong Diamond antifade reagent,

it was chosen as mounting medium of choice. As an advantage, the fluorescent mounting medium did not require long curing after mounting, as the ProLong Diamond antifade reagent did (24h). This allowed for a quicker elution workflow. Also, the fluorescent mounting medium was available in higher quantities and was a more economical choice. These were important qualities in this study where repeated staining of slides was required.

In the original protocol, the final step before coverslipping the slides was the airdrying of samples. This was done to remove all water that may react with the mounting medium. The drying of tissue samples before staining may change the epitopes of the antigens of the tissue remasking them (Boi et al., 2016). This may lead to problems in staining with antibodies having a low recognition of target sites on the tissue. In the original protocol, this posed no problem, since all antibody binding steps had been completed at this point. However, in an elution workflow, the tissue is restained, and no antigen retrieval step is done after the initial antigen retrieval step of the first antibody. The drying of samples could have, thus, in theory, affected the binding of subsequent antibodies. However, no difference was found in the staining of CD20 antibody when the tissue was dried before staining compared to when the tissue was kept moist. Nevertheless, all samples were kept moist during all steps of staining.

6.3 Elution solutions

The elution of bound antibodies has traditionally not been utilized in histology but has been common practice for example in the purification and characterization of antibodies (Gendusa et al., 2014). The SDS pH2 solution was adopted from the work of Pirici et al., 2009 where they reported successful removal of bound primary antibodies and bound primary antibodies detected with a fluorescent secondary antibody from tissue (Pirici et al., 2009). Pirici et al., 2009 had tried different elution solutions with high and low pH-values, high osmolarity and denaturing properties and concluded that SDS pH2 was the best elution solution. They did not report that the SDS pH2 solution would not be effective in removing any of the bound antibodies tested.

The 2-ME/SDS elution solution was adopted from the work of Gendusa et al., 2014 where they also reported successful removal of bound primary antibodies and successful removal of bound primary antibodies detected with a fluorescent secondary antibody (Gendusa et al., 2014). Gendusa et al., 2014 conducted their work after Pirici et al., 2009 and compared the SDS pH2 elution solution with the 2-ME/SDS elution solution. They found that the 2-ME/SDS solution was the most effective elution solution removing all bound antibody, whereas the SDS pH2 solution was not

effective against the antibody with the strongest binding affinity when bound by a secondary antibody. When the strongest antibody was bound to the tissue with no secondary antibody binding to it, the SDS pH2 solution was found to remove all tested antibodies (Gendusa et al., 2014).

In this study, the elution of antibodies was only tested when both primary and secondary antibodies were bound. The results with SDS pH2 elution step conducted in this study are in line with Gendusa et al., 2014 in that the elution did not remove all antibody with VP1 and IgM and their secondary markers staying bound.

The 2-ME/SDS elution protocol differed from the original protocol of Gendusa et al., 2014. This difference was due to different lab equipment available. There was no access to a platform shaker that could have been placed in an incubator to raise the temperature to 56 °C as required for the 2-ME/SDS elution protocol. The hooded platform shaker available had a heater and could reach 60 °C according to the equipment, but in reality, it did not. This was probably due to insufficient insulation of the equipment. Initially, the 2-ME/SDS elution protocol was tested with the heated shaker and preheated solutions but was abandoned when the 2-ME/SDS elution solution was found to work without shaking at 60 °C in a water bath with a stable temperature. Raising the incubation temperature of the 2-ME/SDS solution had drastic effects on the effectiveness of antibody elution. Before raising the temperature of the elution solution, the 2-ME/SDS solution was not at all effective in the removal of bound antibody.

With temperature affecting the elution of antibodies so much for 2-ME/SDS, the ineffectiveness of SDS pH2 solution in the elution of antibodies may also be partially due to low temperatures. The heated shaker was initially operated with the assumption that the temperature displayed on the apparatus matched the temperature under the hood. With the temperature set to 50 °C for SDS pH2 elution, the actual temperature of the shaker was probably lower than this. Had the inaccuracy of the heated shaker been known from the start, the temperature of the shaker could have been raised to higher temperatures to compensate for the heat loss. With all SDS pH2 elution steps done in the heated shaker with an unstable temperature, it is probable that at least part of the inefficiencies of the SDS pH2 elution solution were due to incorrect temperatures. With the discovery of 2-ME/SDS as an efficient elution solution at 60 °C, the SDS pH2 solution was not studied further.

The elution workflow did not affect the staining pattern of the markers. The number of elutions was not limited by the decrease of the fluorescent signal strength nor by the destruction of the sample tissue, but by not having enough relevant antibodies to stain with.

6.4 Counterstaining

The Slidestrider virtual microscopy system used in the study requires a counterstain for tissue recognition. It illuminates the sample with white light and takes an image. This image serves as the starting file for the creation of the tissue map. Other commercial tissue scanners with a fluorescence imaging capability like the Hamamatsu NanoZoomer S60 use darkfield illumination to image the sample for the formation of the preview map (www.hamamatsu.com/resources/pdf/sys/SBIS0043E_NanoZoomers.pdf; 11.01.2019). Using darkfield illumination instead of brightfield illumination enables the creation of a preview map without the need for a brightfield counterstain. Even though a brightfield image of each sample was taken and all samples were scanned using brightfield microscopy in addition to fluorescent microscopy, the Alexa Fluor dyes did not lose their intensity.

Hematoxylin is a very common counterstain for brightfield microscopy. It is reported that hematoxylin quenches the fluorescent signal (Chilosi et al., 1983). This is expected since a dye like hematoxylin blocks light from transmitting to the sample. However, it is also reported that light hematoxylin staining can be used in conjunction with immunofluorescent staining to facilitate accurate whole tissue scanning of fluorescently labeled samples (Isola et al., 2016). In this study, hematoxylin was found to block the fluorescent signal and therefore another counterstain was needed for the tissue scanner to recognize the sample.

Sudan black is generally used for the quenching of autofluorescent background staining of fluorescently stained tissue. For example, quenching of strong autofluorescence by Sudan black is for reported in the pancreatic tissue (Erben et al., 2016) and renal tissue (Zhang et al., 2018). The reason for Sudan black's ability to quench autofluorescence is not known, but it has been speculated that it may emerge from either quenching the excitation wavelength of autofluorescing tissue, or quenching the emission of the emitted autofluoresence signal locally at the autofluorescing sites, without chemically altering the autofluorescing tissue structures (Erben et al., 2016).

The idea for counterstaining tissue with Sudan black emerged from using Sudan black as an agent for quenching autofluorescence of tissue. Sudan black was not incorporated as part of the staining protocols done in this study due to background autofluorescence but rather it had become a standard part of staining protocols performed in the lab. Viewing tissue samples that had a Sudan black incubation step done in the staining revealed a faint blue coloring. This lead to the

idea of using it as a background stain. Searching literature with the terms “Sudan black” and “counterstaining” found no applications of Sudan black used as a counterstaining agent of tissue.

With strong and well established counterstaining agents like hematoxylin and eosin, there has probably not been a need to find new ways of counterstaining tissue. Only in this sort of work where the tissue scanner can only recognize the tissue using brightfield microscopy, does a new method for counterstaining need to be developed. With Sudan black having only a modest staining potential for brightfield imaging, it is no surprise that counterstaining with it has not been reported earlier. The intensity of the Sudan black counterstain develops slowly and the intensity achieved with an 8-10 minute incubation is strong enough for this application. Stronger Sudan black counterstains might have proven troublesome if they had blocked light reaching the fluorophores.

As seen in this study, increasing the concentration of the Sudan black solution from the 0,1% used in the autofluorescence quenching applications to 1,0% used in the counterstain of nPOD tissue samples did not affect the strength of the fluorescence markers on the tissue. The result of this study is both supported and countered by literature. Sudan black is reported to attenuate both autofluorescence and the signal of fluorescent markers with increasing concentrations (Schnell et al., 1999; Zhang et al., 2018). In contrast, Sudan black is also reported to not affect the intensity of fluorescent markers at a concentration of 0,25% (Erben et al., 2016). These conflicting reports may arise from a number of differences in the staining protocol and the Sudan black solutions. According to Erben et. al., 2016 a suitable mounting medium is key to a strong fluorescent signal without autofluorescence. The use of an antifade reagent-free mounting medium is recommended since antifade reagents are reported to react with Sudan black generating autofluorescence (Romijn et al., 1999). Although the fluorescent mounting medium with an antifade reagent was used when counterstaining with a 1,0% Sudan black, there were no indications of autofluorescence or fading of fluorescent signals. The Prolong Diamond mounting medium was not tested when tissue samples were counterstained with 1,0% Sudan black. The interaction of Sudan black solution with mounting mediums was not specifically studied in this work.

The properties of Sudan black’s absorption and emission spectra shed light into why even the stronger 1,0% Sudan black solution used in this study may not have caused problems in the detection of the fluorescent signal. Sudan black has been reported to cause autofluorescence in the far red wavelengths (Whittington & Wray, 2017) and this is evident from Sudan black’s emission peak wavelength of 660 nm in ethanol (Zakerhamidi et al., 2015). In this study, Sudan black was diluted in ethanol. Since no fluorescent markers were used that emitted light at those long

wavelengths and since no filter cube was available in the virtual microscopy system for the detection of those longer wavelengths, the emission spectra of Sudan black autofluorescence was not detected in the study. The absorption spectra of Sudan black is at its lowest at the shorter visible wavelengths and peaks at 597,5 nm (Zakerhamidi et al., 2015). The staining with rabbit anti-human antibodies that would have used Alexa Fluor 568 secondary antibodies was not tested when the stronger concentration of Sudan black was used. Since the absorption spectra of Sudan black is close to the emission spectra of Alexa Fluor 568, the stronger Sudan black solution may have made the red fluorescent signal fainter. If double staining using the cocktail method is to be pursued with future stainings, the effect of the stronger Sudan black counterstain on the Alexa Fluor 568 marker should be studied.

During the initial setting up of the fluorescent multistaining protocol, high levels of autofluorescence originating from erythrocytes was present even though the stainings included a Sudan black staining step to reduce the autofluorescence signal. The final protocol used for staining the nPOD tissue samples used a 10 fold stronger Sudan black solution than the initial solution used. Even with this dramatic increase in the concentration of Sudan black, the autofluorescence signal of erythrocytes in the spleen tissue was not diminished. This seemed counterintuitive since the autofluorescence quenching ability of Sudan black is reported to increase with higher concentrations (Zhang et al., 2018). It is also reported that although Sudan black is widely used to remove autofluorescence, it is not very effective against the autofluorescence caused by erythrocytes (Whittington & Wray, 2017).

6.5 Virtual microscopy

The development of virtual microscopy has been rapid with many commercial tissue scanners emerging capable of scanning fluorescently labeled images (Buscone et al., 2014). The upsides of virtual microscopy are many. Fluorescent markers lose their signal with time, with the time depending on the mounting medium and the type of fluorescent marker used (Burry, 2010d). Fluorescent markers are also sensitive to lasers, losing their signal strength with repeated viewings (Burry, 2010b). A virtual whole tissue scan, on the other hand, does not lose its signal and can be viewed multiple times (Al-Janabi et al., 2012). The tissue is also easy to view on a computer screen and does not require spending time in dark rooms suitable for fluorescent imaging (Ghaznavi et al., 2013). Altering the field of view quickly and marking regions of interest are other upsides of viewing a whole slide virtual scan compared to analyzing a entire tissue sample under the microscope

(Higgins, 2015). Accurate navigation of the whole slide scan using the arrow keys of the computer gives a more reliable result of the positivity present on the sample. This was especially important in a study like this where single positive cells need to be found on a large tissue sample. In regards to this study, searching for VP1 positivity under the microscope would have been impossible. The relocation of the VP1 positive spot, from which VP1 positivity was stripped with the elution solution, would have been even more difficult for the subsequent imaging of the other markers used.

Generating multiple overlapping whole tissue scans of the same sample stained with different antibodies was the initial goal of the study. However, the imaging of the whole slide for each antibody stained was abandoned after multiple rounds of testing the scanning of fluorescently labeled tissue samples. The problems facing multiple imaging of the same slide were various. Some of the problems were solvable, but many were inherent of the virtual microscope apparatus and could not be overcome.

Tissue scanning is sensitive to dust, debris and air bubbles on the sample which are especially prone to be deposited when manually staining and coverslipping the slides. This can sometimes be overcome using the scanning software to limit the depth of the automatic searching of the focus plane and by adjusting focus point distance. However, due to limitations in the Observer software, this could not be done. The difficulties with accurate focusing not only lead to debris being a bigger problem in scanning but also made the scanning of slides with no debris very difficult.

The problems in the preview map formation lead to inaccurate scanning. Although the composing of accurate preview maps depends mainly on good quality tissue that can be recognized, the quality of tissue samples was not what made preview map creation problematic. In Figure 9A the inaccurate preview map did not result from differences in tissue morphology since there was no difference in the tissue where the tiles were scanned compared to where they were not scanned. A problem like this is difficult if not impossible to solve by adjusting the parameters of map creation. In many cases adjusting preview map parameters such as the size of the tissue to be detected or the threshold strength of tissue recognition helped in tissue recognition. However, the Observer software did not function consistently and finding suitable values for scanning did not aid tissue recognition in the long term.

Had problems with focal plane selection and tissue recognition been solved, the scanning of the entire tissue sample and overlaying of subsequently scans would still have been very challenging. Differences in the position of loaded slides on the microscope table lead to misalignments in subsequent scanning. Slight misalignments of the scan could probably have been

fixed in an image editing software, but more drastic misalignments where the scanned tissue does not fit preview map like in Figure 9D are not fixable. Differences in slide position on the microscope table are expected, but the differences between slides are drastic with the Slidestrider. This may be due partly to parts of the scanner jamming, and loosening as a result.

Although the Slidestrider is meant to be an automatic scanner, the mounting problems meant that constant supervision was required for successful scans. These problems combined with a myriad of random and unpredictable problems like sudden misalignment of filter cubes, the constant crashing of the program and occasional breaking of slides by the slide loader arm forced a change in protocol.

Even though the tissue scanner did not work in an anticipated way and the approach for conducting this study had to be changed, the results gained would not have been attainable without the tissue scanner. Having a map of the tissue with the VP1 positivity marked allowed quicker searching of the positive sites for reimaging with a x 40 lens. For an unknown reason, the coordinates of the imaging sites noted within the Objective Imaging Surveyor software did not stay the same between stainings, even though coordinates of the slide were synchronized between loads on the slide table by using a corner of the slide as an origo. Due to inaccuracies in the coordinates, the coordinates were used to give a rough estimate of the location, and the final imaging location was found using the DAPI channel to align the field of view with the DAPI-channel of the VP1 positive image.

DAPI signal has been used as the basis for aligning images taken from multiplexed tissue samples with the aid of software such as the TurboReg ImageJ Fiji plugin (Bolognesi et al., 2017). The approach taken in this study to align the images taken of the nPOD tissue samples was also based on the presence of the DAPI signal, but the images were aligned manually. The subsequent images taken of the VP1 positive locations aligned quite well, but exact aligning of the field of view with the initial VP1 positive image's DAPI channel was not possible using the system. The fine tune alignment of images was done using Adobe Photoshop.

During the process of aligning the nuclei, the importance of the focal plane of scanning showed its importance. Slight differences in focal plane lead to slightly different shapes and alignments of the nuclei, especially of the nuclei of the blood vessels. These slight misalignments were not a hindrance to the accurate alignment of the fluorescent channels in the images, with the nuclei matching mostly almost perfectly on top of one another. However, aligning entire tissue scans with one another may have proven difficult with more substantial misalignments forming. This may

have been solved by Z-axis scanning of the tissue sample that was not available with the Slidestrider using the Observer software. However, with the update of the Slidestrider software after the completion of this work, the Z-scanning of fluorescent tissue samples became available. The merging of subsequently imaged whole slide samples has been done successfully using the Hamamatsu NanoZoomer S60 (Bolognesi et al., 2017).

Z-stack scanning of tissue samples would have allowed more accurate imaging of VP1 positive cells. Often the VP1 positive cell was slightly out of focus in the whole tissue scans used to locate VP1 positivity on the tissue sample. This did not hinder the searching of these cells, but the quality of the scanned tissue would not have been high enough to be used in the final merged images. If merging whole tissue scans is to be pursued in the future, Z-axis depth of the scanned tissue could make the aligning of scans and attaining of quality snapshots of tissue possible.

One of the aims of this study was to create a workflow for the sequential staining of samples and aligning the sequentially stained whole tissue samples to create a file where colocalization of fluorescent signals could be visualized. This aim was partially achieved with an elution workflow facilitating the multiple staining of tissue samples. However, scanning whole tissue for each marker stained for was not feasible, and the imaging of regions of interest had to be done manually. No other parts of the tissue besides the regions of interest were imaged in the final study design. This limits the application of the data gathered to only this study, whereas aligning the whole tissue scans of multiple markers could have opened new research directions in the future. Studying the presence and colocalization of multiple markers tissue-wide could have been useful in a wide range of studies not limited to enterovirus research. With new research ideas, additional markers could have been stained for and the scans of these stainings could have been added to the stacked library of scans from that sample. The 2-ME/SDS elution method has been reported not to affect the binding of antibodies to antigens even with multiple rounds of staining (Bolognesi et al., 2017) and if an antibody cocktail method is used for staining, the amount of staining rounds is halved.

6.6 Locating enterovirus-positive cells in the nPOD spleen samples with VP1 antibody and staining the samples with multiple markers

The spleen has been very limitedly studied for its EV positivity. A higher correlation of VP1 positivity in the spleen of T1D patients and AAb+ patients has been found when compared to controls in chromogenic stainings using VP1 clone 5D8/1 (M. Oikarinen et al., 2018). When staining the test

spleens before the nPOD spleen samples, almost no VP1 positivity was found. However, the test spleens stained with VP1 were not as thoroughly searched for EV positivity as the nPOD spleen samples were.

The VP1 antibody had been used in previous applications with a 1 h incubation at room temperature (Saarinen et al., 2018) and for consistency, these same parameters were used in this study as well. Spotting VP1 positive cells was only possible by scanning the sample stained with a Sudan black counterstain and carefully searching the virtual microscopy image for positivity. Imaged VP1 positive locations on the scanned tissue were analyzed individually and graded for their positivity. With VP1 positivity showing only in individual cells or parts of cells with clear borders, the VP1 positivity was determined to be genuine and not as unspecific background signal. The smallest and faintest positivity sites were disregarded since they could not safely be regarded as correct positivity. The results for the colocalization of VP1 was very limited in this study due to the low sample number. The results may be somewhat skewed because around half of the VP1 positive cells were found on a single sample with the rest of the positivity spread between the other samples (Table 2). Although the amount of VP1 positive cells was minimal, clear positivity was found on all samples studied except for one.

EV VP1 antibody (clone 5-D8/1) is widely used for the detection of EVs (Ettischer-Schmid et al., 2016; Krogvold et al., 2015; M. Oikarinen et al., 2018; Richardson et al., 2009). However, 5-D8/1 is known to bind unspecifically with smooth muscle tissue (Richardson et al., 2009), which is a likely explanation for the VP1 staining of blood vessels seen in this study (data not shown). This antibody is also reported to interact with common cellular proteins (Ettischer-Schmid et al., 2016; Hansson et al., 2013) under some instances. However, the unspecific positivity that was seen in the staining done by Ettischer-Schmid et al., 2016 was spread over a large area (Ettischer-Schmid et al., 2016) and differed drastically from the single cell positivity seen in this study. The work by Ettischer-Schmid et al., 2016 was mainly concentrated on staining heart tissue (Ettischer-Schmid et al., 2016) and this large unspecific scale tissue staining has not been reported by other studies to the knowledge of the author of this study.

Nonetheless, to be sure of genuine VP1 positivity in future spleen stainings, the staining with VP1 (clone 5-D8/1) could be complemented with other existing EV antibodies. The novel rat CV-B1 VP1 monoclonal antibody 3A6 was recently published (Saarinen et al., 2018). 3A6 has been reported to stain for VP1 without unspecific background staining of the smooth muscle

tissue (Saarinen et al., 2018). However, based on initial results, this antibody may not be sensitive enough to be used for staining for VP1 in the spleen (unpublished data).

Although most VP1 positive cells had some colocalization with the other tissue markers stained for, the cells did not often have a clear marker that would have colocalized entirely with the VP1 positive area. Also, markers scarcely completely stained the cell where VP1 positivity was present. Even when most of the VP1 positive area had colocalized with a marker, often CD3, the signal of the marker at that location was a lot fainter than in other cells found around the VP1 positive cell. This may be due to enteroviruses hindering transcription of the host cell's genes and cleaving of the cellular translation initiation factor 4 gamma 1 (eIF4G) with their enteroviral proteases 2A and 3C (Olli H. Laitinen et al., 2016). By doing this, the virus can harness the cellular machinery for the production of viral particles (Olli H. Laitinen et al., 2016). Another possibility for lower host protein expression in VP1 positive cells is the action of PKR, a type I IFN and dsRNA-activated protein with antiviral activity. This antiviral activity also leads to a general inhibition of translation within a cell, thus also lowering host protein expression (Garcia et al., 2006). This study may also have missed the cell markers that would have given a strong colocalizing signal with VP1 positive cells. The varying morphology of the VP1 positive cells indicates that there are multiple cell types present with VP1 positivity. This is also supported by the fact that the different markers stained for all colocalized with VP1 to some extent.

VP1 was seen to stain blood vessels in this study faintly. Interestingly the mature dendritic cell marker CD83 also stained blood vessels in a similar pattern and the VP1 and CD83 signals colocalized. The CD83 signal in the blood vessels was also very weak (data not shown). In light of the reported unspecific staining of smooth muscle by VP1, the colocalization of weak CD83 signal with the VP1 positivity in the blood vessels may not be genuine colocalization. The $CD83^{+}$ cells observed could be due to long exposure times needed to visualize the positivity. The data in regards to CD83 stainings, in general, may be unreliable since only part of the samples were stained with it and the antibody had passed its expiration date. Only five of the nine nPOD spleen samples were stained with CD83 because there was not enough antibody for the staining of all the samples. Staining the tissue samples with a fresh CD83 antibody would be needed to draw conclusions about the colocalization of VP1 with CD83 signal.

The determination of signal colocalization is not straight forward and may be subject to error resulting from the imaging of markers. When imaging sequentially stained markers, the focal plane of imaging is bound to change. In this study, the focal plane was adjusted manually for

each region of interest, and the focal plane depth was determined by the sharpness of the marker imaged. With markers imaged at different focal planes, the location of positivity relative to other images may shift. The shift is slight at best, as can be seen when aligning the DAPI stained nuclei of the images. Since the shift is minor, it could cause false positive or false negative colocalization in cases where only part of the signal colocalized with VP1. It would not affect instances where most or all of the VP1 signal colocalized with another marker.

Another common problem with regards to colocalization is having different cells on top of one another in the field of view. In this case, colocalization of signals is observed although the signals are in separate cells and are not truly originating from the same location. This phenomenon may explain some of the partial colocalizations of signals seen in this study. A VP1 positive cell in the middle of a follicle or PALS may be partially $CD20^+$ or $CD3^+$, resulting from $CD20^+$ and $CD3^+$ cells surrounding the VP1 positive cell. This phenomenon could explain why many $CD20^+$ cells partially colocalize with VP1 but why no complete or near complete colocalization is seen. However, it cannot be ruled out either that the colocalization is true.

One aim of the study was to find VP1 positive cells in the nPOD spleen samples and determine the cell type of these cells. VP1 positivity was found in eight out of nine samples studied, and since a sequential staining protocol was functional, the restaining of the tissue sections was possible. This made possible the creation of images with colocalizing fluorescent signals and VP1 was found to colocalize with all markers stained for.

Although spleen sections from organ donors with T1D and non-diabetic donors were studied, no conclusions can be drawn about the VP1 positivity in different cell types between the donor groups. The numbers in donors and sections studied and in cells positive for VP1 were too small.

6.7 Possible additional stainings

Assigning VP1 positivity to a compartment of the spleen was not always straightforward. In some cases, VP1 positivity was seen in between compartments without a clear border. In addition to the broad compartments defined in this study, a more detailed mapping of compartments could be done in future studies with additional markers. The morphology of the spleen could be better visualized with a CD271 staining. CD271 stains fibroblastic reticulum cells and follicular dendritic cells. Both cell types are resident cells with fibroblastic reticulum cells making up the connective tissue in PALS whereas follicular dendritic cells support the follicle (Steiniger et al., 2018). Also, the

borders of the PALS and follicles could be visualized with either smooth muscle α-actin (SMA) or MAdCAM-1 (Steiniger, 2015). The stromal cells surrounding the PALS and the follicles stain positive for both markers and do not stain for CD271. If CD271 staining is to be done, it has to be stained for last since the chromogenic stain cannot be washed off and no further stainings could be done.

Since the sample size in this study was not large, the best course of action for further investigations may be to stain more samples with the same markers used in this study before staining with other markers. However, In light of the initial results gained in the study, future stainings could be done dividing the $CD3^+$ T cells to $CD4^+$ and $CD8^+$ subsets, since CD3 colocalized with VP1 quite often. A subset of macrophages, T cell receptor macrophages, are also $CD3^+$ (Chávez-Galán et al., 2015). Further differentiating the $CD20^+$ B cells to the $CD27^+$ subset may not be as interesting, since VP1 signal did not fully colocalize with the CD20 signal. On the other hand, staining for CD27 might be interesting for gaining a better image of the morphology of the follicle, since the periphery of the follicle is $CD27^+$ (Steiniger, 2015). The colocalization of neutrophils with VP1 could be studied with the CD177 antibody, as its signal was clear in the spleen in optimization stainings. Neutrophils have been found surrounding the follicle and having an activator role for B cells, making them a possible target (Bai et al., 2017). Only small quantities of the macrophage marker CD163 and the neutrophil marker CD177 were available, and thus the nPOD samples were not stained with them.

The staining for macrophage subsets is challenging since multiple subsets exist and markers stain across many subsets (Chávez-Galán et al., 2015). To make things more complicated, the macrophage subsets are defined in mice, where most of the information with regards to spleen has been gained, whereas in humans the subsets are not nearly as well defined (Murray & Wynn, 2011). The mouse spleen contains resident marginal metallophilic macrophages and marginal zone macrophages that are not found in humans (Steiniger, 2015). The marginal metallophilic macrophages are located in the marginal sinus, a blood-filled compartment around the PALS and the follicles that is missing in humans. Marginal zone macrophages are macrophages found in the mouse marginal zone. The marginal zone is difficult to define in humans and is mainly a B cell compartment around the follicles. Although no clear counterpart for these macrophages can be found in humans, macrophages are present at the follicular periphery and around capillary sheats in humans, that may have similar functions. These two macrophage subtypes in mice are of interest since they are $CD169^+$ (Steiniger, 2015). $CD169^+$ macrophages have been speculated as having a role in immunological tolerance by lessening self-antigen responses (Chávez-Galán et al., 2015). Since

T1D is an autoimmune disease, this link is of interest. $CD169^+$ macrophages have also been associated as mediators of the immune response against viruses, producing type I IFN and recruiting natural killer cells to the rat spleen (Chávez-Galán et al., 2015). In the human spleen, $CD169^+$ macrophages have been found around capillary sheaths (Steiniger, 2015). In conclusion, although dividing the human spleen macrophages into subsets is difficult, staining with the CD169 marker could be of interest. As staining with the CD163 works in the spleen, it is also a marker of interest, since it can help differentiate red pulp macrophages from follicular and capillary sheath macrophages, as discussed in the Review of the literature ("Spleen lymphocyte markers"). Distinctions in the macrophage populations can also be made with the Fc-γ receptors, with which the red pulp macrophages can be distinguished (Nagelkerke et al., 2018).

A logical immune cell type that could be VP1 positive in the spleen are dendritic cells since they act as professional antigen presenting cells for T cells activating the immune response against viruses (Freer & Matteucci, 2009). Also, dendritic cells are particularly interesting in the context of T1D, since they play a vital role in the disease progression by activating the disease progress and maintaining disease progression (Morel, 2013). Dendritic cells present in the pancreas take up self-antigens against the beta-cells of the spleen and present them in the lymph nodes to T cells, which then infiltrate the pancreas destroying the beta-cells in the islands of Langerhans (Morel, 2013).

With no marker in this study showing a strong and complete colocalization with VP1, it is compelling to test dendritic cell markers more thoroughly. Staining with a fresh CD83 mature dendritic cell marker is of interest since faint colocalization of the signal was observed. However, staining with the CD83 marker is not enough to distinguish $CD83^+$ dendritic cells from B and T cells that both express CD83 as well (Aerts-Toegaert et al., 2007). Differentiating dendritic cells into their subsets is difficult. Myeloid dendritic cells express CD11c, CD11b, CD13 and CD33 with monocytes also expressing CD11c (Collin et al., 2013). Splitting the myeloid dendritic cells further into subsets becomes tricky since the two fractions express CD1c and CD141 (Collin et al., 2013), of which CD141 is also expressed by the splenic sinus endothelia (Steiniger, 2015). Plasmacytoid dendritic cells are easier to distinguish by staining for either CD123, CD303 or CD304 (Collin et al., 2013). Another subset to stain for are $CD14^+$ dendritic cells. All of these dendritic cell types are found in the lymph nodes, but differentiating between resident cells and cells migrating from the other tissues is difficult. Human dendritic cells do not stain for CD3 and CD20 markers (Collin et al., 2013). In addition to staining with CD83, further stainings could be done with one of the plasmacytoid

dendritic cell markers and CD11b, CD1c and CD14 giving an overview of the different dendritic cell subsets.

6.8 Future perspectives

With a successful elution protocol in place, future studies of tissue samples with multiple markers are possible. In this study, the number of markers was limited (N=5) and could be stained consecutively using the single staining protocol. Future studies with more markers may need to test double staining protocols again for less labor intensive staining protocols. With the current setup, the imaging of samples is also laborious, and may not lend itself to other studies where broader areas of tissue instead of individual virus-positive cells need to be imaged. Also, if many VP1 positive locations are found on slides and the number of slides is high, manually imaging each location for each marker will prove difficult.

Since the completion of the study the software of the Slidestrider has been updated and this may make the scanning and stacking of whole tissue scans more feasible. The update has made the software more reliable, and it can now facilitate the scanning of tissue sections with a Z-stack. This could prove very useful for attaining in-focus images of VP1 positive cells, possibly making additional manual imaging of VP1 positive locations unnecessary. Although the scanner hardware has not changed, the problems with misalignments of slides may be overcome by imaging the whole slide for each marker. Although this makes the scanning take longer, no preview map would be needed and misalignments could be fixed manually. However, the aligning of whole tissue scans may not be possible with the software available, and custom software may need to be made. If another tissue scanner such as the Hamamatsu NanoZoomer S60 is acquired, Sudan black counterstaining is no longer required and possible problems with Sudan black autofluorescence can be disregarded.

If whole tissue scans of multiple markers are attained in the future, this could open up ways of analyzing the samples beyond what was feasible in this study. Modern tools utilizing algorithms could easily give an accurate analysis of the tissue-wide distribution of a multitude of markers. In addition, the elution and scanning workflow could be applied to other tissues of interest such as the pancreas or the intestine. This could build a more complete picture of the presence of EV-positive cells in the tissues of T1D donors, AAb+ donors, and non-diabetic control donors. Analyzing these larger data sets could further elaborate on the role of EVs and spleen in the initiation and progression of T1D.

7 Conclusions

This study aimed at setting up an elution workflow for the whole slide imaging of spleen tissue samples from the nPOD tissue bank. Various antibody staining methods were tested. These included both single staining and double staining protocols. The double staining protocols tested were the antibody cocktail staining and the Fab-fragment protocol, where the Fab-fragment was used as a blocking step in the staining. Neither double staining method proved effective for this study, and the single staining method was used for the staining of the nPOD spleen samples. Single staining of antibodies is laborious. In this study, the number of markers was limited (N=5), so the staining did not prove too burdensome. However, staining for a higher number of antibodies in the future would require the staining of multiple markers at once. Setting up an effective elution workflow was successful in this study with the use of 2-ME/SDS elution solution. This elution solution can be used in future elution protocols for the spleen and likely for other tissues of interest as well.

Initially, this study aimed at attaining whole slide tissue scans of the spleen samples for each marker stained for. Due to technical difficulties, this strategy was abandoned, and the virtual microscope system was instead used as a tool to locate the VP1 positive sites on the tissue for manual imaging. This method was somewhat laborious, but fulfilled the objective of staining and imaging the VP1 positive locations for lymphocyte markers. The imaged attained were combined into one image where the colocalization of VP1 could be studied. Because whole-slide scans of each marker were not attained, further studies of the morphology of these VP1 positive spleen samples was not possible. Using the virtual microscopy system to find VP1 positive locations for reimaging manuallyiis probably not a feasible strategy for future stainings, and a strategy for whole slide scanning of the slide for each marker needs to be established.

VP1 signal was punctual and followed the outline of individual cells. Cells were found to be either partially or entirely VP1 positive and the morphology of VP1 positive cells varied. VP1 positive cells were found in different areas of the spleen. Only two of the 21 VP1 positive cells did not colocalize with any of the markers studied. VP1 colocalized most with CD3 and CD68 markers and to a lesser degree with CD20.

References

Aerts-Toegaert, C., Heirman, C., Tuyaerts, S., Corthals, J., Aerts, J. L., Bonehill, A., … Breckpot, K. (2007). CD83 expression on dendritic cells and T cells: Correlation with effective immune responses. *European Journal of Immunology*, *37*(3), 686–695. https://doi.org/10.1002/eji.200636535

Åkerblom, H. K., Vaarala, O., Hyöty, H., Ilonen, J., & Knip, M. (2002). Environmental factors in the etiology of type 1 diabetes. *American Journal of Medical Genetics*, *115*(1), 18–29. https://doi.org/10.1002/ajmg.10340

Al-Janabi, S., Huisman, A., & Van Diest, P. J. (2012). Digital pathology: current status and future perspectives. *Histopathology*, *61*(1), 1–9. https://doi.org/10.1111/j.1365-2559.2011.03814.x

Bai, M., Grieshaber-Bouyer, R., Wang, J., Schmider, A. B., Wilson, Z. S., Zeng, L., … Nigrovic, P. A. (2017). CD177 modulates human neutrophil migration through activation-mediated integrin and chemoreceptor regulation. *Blood*, *130*(19), 2092–2100. https://doi.org/10.1182/blood-2017-03-768507

Baidal, D. A., Sanchez, J., Alejandro, R., Blaschke, C. E., Hirani, K., Matheson, D. L., … Ricordi, C. (2018). *POSEIDON study: a pilot, safety and feasibility trial of high-dose omega 3 fatty acids and high-dose cholecalciferol supplementation in type 1 diabetes*. *CellR4* (Vol. 6). Retrieved from https://www.cellr4.org/wp-content/uploads/sites/2/2018/04/2018-03-POSEIDON-Protocol-Consent-Assent-2.pdf

Beyerlein, A., Chmiel, R., Hummel, S., Winkler, C., Bonifacio, E., & Ziegler, A.-G. (2014). Timing of Gluten Introduction and Islet Autoimmunity in Young Children: Updated Results From the BABYDIET Study: Table 1. *Diabetes Care*, *37*(9), e194–e195. https://doi.org/10.2337/dc14-1208

Blauwet, L. A., & Cooper, L. T. (2010). Myocarditis. *Progress in Cardiovascular Diseases*, *52*(4), 274–288. https://doi.org/10.1016/J.PCAD.2009.11.006

Boi, G., Scalia, C. R., Gendusa, R., Ronchi, S., & Cattoretti, G. (2016). Disaccharides Protect Antigens from Drying-Induced Damage in Routinely Processed Tissue Sections. *Journal of Histochemistry & Cytochemistry Cytochemistry*, *64*(1), 18–31. https://doi.org/10.1369/0022155415616162

Bolognesi, M. M., Manzoni, M., Scalia, C. R., Zannella, S., Bosisio, F. M., Faretta, M., & Cattoretti, G. (2017). Multiplex Staining by Sequential Immunostaining and Antibody Removal on Routine Tissue Sections. *Journal of Histochemistry & Cytochemistry*, *65*(8), 431–444. https://doi.org/10.1369/0022155417719419

Bolte, S., & Cordelières, F. P. (2006). A guided tour into subcellular colocalization analysis in light microscopy. *Journal of Microscopy*, *224*(3), 213–232. https://doi.org/10.1111/j.1365-2818.2006.01706.x

Boltjes, A., & van Wijk, F. (2014). Human Dendritic Cell Functional Specialization in Steady-State and Inflammation. *Frontiers in Immunology*, *5*, 131. https://doi.org/10.3389/fimmu.2014.00131

Breloer, M., & Fleischer, B. (2008). CD83 regulates lymphocyte maturation, activation and homeostasis. *Trends in Immunology*, *29*(4), 186–194. https://doi.org/10.1016/J.IT.2008.01.009

Buchwalow, I. B., & Böcker, W. (2010a). A Picture Is Worth a Thousand Words. In *Immunohistochemistry: Basics and Methods* (pp. 129–139). Berlin, Heidelberg: Springer Berlin Heidelberg. https://doi.org/10.1007/978-3-642-04609-4_14

Buchwalow, I. B., & Böcker, W. (2010b). Multiple Immunofluorescence Staining. In

Immunohistochemistry: Basics and Methods (pp. 69–76). Berlin, Heidelberg: Springer Berlin Heidelberg. https://doi.org/10.1007/978-3-642-04609-4_8

Buchwalow, I. B., & Böcker, W. (2010c). Multiple Multicolor Immunoenzyme Staining. In *Immunohistochemistry: Basics and Methods* (pp. 61–67). Berlin, Heidelberg: Springer Berlin Heidelberg. https://doi.org/10.1007/978-3-642-04609-4_7

Buchwalow, I. B., & Böcker, W. (2010d). Working with Antibodies. In *Immunohistochemistry: Basics and Methods* (pp. 31–39). Berlin, Heidelberg: Springer Berlin Heidelberg. https://doi.org/10.1007/978-3-642-04609-4_4

Burry, R. W. (2010a). Application Methods. In *Immunocytochemistry* (pp. 65–77). New York, NY: Springer New York. https://doi.org/10.1007/978-1-4419-1304-3_7

Burry, R. W. (2010b). Fluorescent Microscopy and Imaging. In *Immunocytochemistry* (pp. 139–149). New York, NY: Springer New York. https://doi.org/10.1007/978-1-4419-1304-3_13

Burry, R. W. (2010c). Labels for Antibodies. In *Immunocytochemistry* (pp. 55–64). New York, NY: Springer New York. https://doi.org/10.1007/978-1-4419-1304-3_6

Burry, R. W. (2010d). Single Antibody Procedure. In *Immunocytochemistry* (pp. 97–110). New York, NY: Springer New York. https://doi.org/10.1007/978-1-4419-1304-3_10

Buscone, S., Argentieri, M. C., Pilla, D., & Cattoretti, G. (2014). Whole-slide, Quadruple Immunofluorescence Labeling of Routinely Processed Paraffin Sections. *Applied Immunohistochemistry & Molecular Morphology*, *22*(4), e1–e7. https://doi.org/10.1097/PAI.0b013e31829928e7

Camparo, P., Egevad, L., Algaba, F., Berney, D. M., Boccon-Gibod, L., Compérat, E., … Varma, M. (2012). Utility of whole slide imaging and virtual microscopy in prostate pathology. *APMIS*, *120*(4), 298–304. https://doi.org/10.1111/j.1600-0463.2011.02872.x

Chapman, N. M., Coppieters, K., von Herrath, M., & Tracy, S. (2012). The microbiology of human hygiene and its impact on type 1 diabetes. *Islets*, *4*(4), 253–261. https://doi.org/10.4161/isl.21570

Chávez-Galán, L., Olleros, M. L., Vesin, D., & Garcia, I. (2015). Much More than M1 and M2 Macrophages, There are also CD169(+) and TCR(+) Macrophages. *Frontiers in Immunology*, *6*, 263. https://doi.org/10.3389/fimmu.2015.00263

Chilosi, M., Pizzolo, G., & Vincenzi, C. (1983). Haematoxylin counterstaining of immunofluorescence preparations. *Journal of Clinical Pathology*, *36*(1), 114–115. Retrieved from https://jcp.bmj.com/content/36/1/114.long

Chistiakov, D. A., Killingsworth, M. C., Myasoedova, V. A., Orekhov, A. N., & Bobryshev, Y. V. (2017). CD68/macrosialin: not just a histochemical marker. *Laboratory Investigation*, *97*(1), 4–13. https://doi.org/10.1038/labinvest.2016.116

Collin, M., McGovern, N., & Haniffa, M. (2013). Human dendritic cell subsets. *Immunology*, *140*(1), 22–30. https://doi.org/10.1111/imm.12117

Coons, A. H., Creech, H. J., & Jones, R. N. (1941). Immunological Properties of an Antibody Containing a Fluorescent Group. *Experimental Biology and Medicine*, *47*(2), 200–202. https://doi.org/10.3181/00379727-47-13084P

Coons, A. H., Leduc, E. H., & Connolly, J. M. (1955). Studies on antibody production. I. A method for the histochemical demonstration of specific antibody and its application to a study of the hyperimmune rabbit. *The Journal of Experimental Medicine*, *102*(1), 49–60. Retrieved from http://jem.rupress.org/content/102/1/49.long

DiMeglio, L. A., Evans-Molina, C., & Oram, R. A. (2018). Type 1 diabetes. *The Lancet*, *391*(10138), 2449–2462. https://doi.org/10.1016/S0140-6736(18)31320-5

Dotta, F., Censini, S., van Halteren, A. G. S., Marselli, L., Masini, M., Dionisi, S., … Marchetti, P.

(2007). Coxsackie B4 virus infection of beta cells and natural killer cell insulitis in recent-onset type 1 diabetic patients. *Proceedings of the National Academy of Sciences*, *104*(12), 5115–5120. https://doi.org/10.1073/pnas.0700442104

Erben, T., Ossig, R., Naim, H. Y., & Schnekenburger, J. (2016). What to do with high autofluorescence background in pancreatic tissues - an efficient Sudan black B quenching method for specific immunofluorescence labelling. *Histopathology*, *69*(3), 406–422. https://doi.org/10.1111/his.12935

Ettischer-Schmid, N., Normann, A., Sauter, M., Kraft, L., Kalbacher, H., Kandolf, R., … Klingel, K. (2016). A new monoclonal antibody (Cox mAB 31A2) detects VP1 protein of coxsackievirus B3 with high sensitivity and specificity. *Virchows Archiv: European Journal of Pathology*, *469*(5), 553–562. https://doi.org/10.1007/s00428-016-2008-8

Etzerodt, A., & Moestrup, S. K. (2013). CD163 and inflammation: biological, diagnostic, and therapeutic aspects. *Antioxidants & Redox Signaling*, *18*(17), 2352–2363. https://doi.org/10.1089/ars.2012.4834

Franzusoff, A., Redding, K., Crosby, J., Fuller, R. S., & Schekman, R. (1991). Localization of components involved in protein transport and processing through the yeast Golgi apparatus. *The Journal of Cell Biology*, *112*(1), 27–37. Retrieved from http://jcb.rupress.org/content/112/1/27.long

Freer, G., & Matteucci, D. (2009). Influence of Dendritic Cells on Viral Pathogenicity. *PLOS Pathogens*, *5*(7), e1000384. https://doi.org/10.1371/journal.ppat.1000384

Gamble, D. R., Kinsley, M. L., FitzGerald, M. G., Bolton, R., & Taylor, K. W. (1969). Viral antibodies in diabetes mellitus. *British Medical Journal*, *3*(5671), 627–630. Retrieved from https://www.ncbi.nlm.nih.gov/pmc/articles/PMC1984442/pdf/brmedj02049-0045.pdf

Gamble, D. R., & Taylor, K. W. (1969). Seasonal incidence of diabetes mellitus. *British Medical Journal*, *3*(5671), 631–633. Retrieved from https://www.ncbi.nlm.nih.gov/pmc/articles/PMC1984393/pdf/brmedj02049-0049.pdf

Garcia, M. A., Gil, J., Ventoso, I., Guerra, S., Domingo, E., Rivas, C., & Esteban, M. (2006). Impact of Protein Kinase PKR in Cell Biology: from Antiviral to Antiproliferative Action. *Microbiology and Molecular Biology Reviews*, *70*(4), 1032–1060. https://doi.org/10.1128/MMBR.00027-06

Gendusa, R., Scalia, C. R., Buscone, S., & Cattoretti, G. (2014). Elution of High-affinity (>10-9 KD) Antibodies from Tissue Sections: Clues to the Molecular Mechanism and Use in Sequential Immunostaining. *Journal of Histochemistry and Cytochemistry*, *62*(7), 519–531. https://doi.org/10.1369/0022155414536732

Gerdes, M. J., Sevinsky, C. J., Sood, A., Adak, S., Bello, M. O., Bordwell, A., … Ginty, F. (2013). Highly multiplexed single-cell analysis of formalin-fixed, paraffin-embedded cancer tissue. *Proceedings of the National Academy of Sciences of the United States of America*, *110*(29), 11982–11987. https://doi.org/10.1073/pnas.1300136110

Ghazarian, L., Diana, J., Simoni, Y., Beaudoin, L., & Lehuen, A. (2013). Prevention or acceleration of type 1 diabetes by viruses. *Cellular and Molecular Life Sciences*, *70*(2), 239–255. https://doi.org/10.1007/s00018-012-1042-1

Ghaznavi, F., Evans, A., Madabhushi, A., & Feldman, M. (2013). Digital Imaging in Pathology: Whole-Slide Imaging and Beyond. *Annual Review of Pathology: Mechanisms of Disease*, *8*(1), 331–359. https://doi.org/10.1146/annurev-pathol-011811-120902

Gillespie, K. M., Bain, S. C., Barnett, A. H., Bingley, P. J., Christie, M. R., Gill, G. V, & Gale, E. A. (2004). The rising incidence of childhood type 1 diabetes and reduced contribution of high-risk HLA haplotypes. *The Lancet*, *364*(9446), 1699–1700. https://doi.org/10.1016/S0140-6736(04)17357-1

Hansson, S. F., Korsgren, S., Pontén, F., & Korsgren, O. (2013). Enteroviruses and the pathogenesis of type 1 diabetes revisited: cross-reactivity of enterovirus capsid protein (VP1) antibodies with human mitochondrial proteins. *The Journal of Pathology*, *229*(5), 719–728. https://doi.org/10.1002/path.4166

Harris, K. G., & Coyne, C. B. (2013). Enter at your own risk: how enteroviruses navigate the dangerous world of pattern recognition receptor signaling. *Cytokine*, *63*(3), 230–236. https://doi.org/10.1016/j.cyto.2013.05.007

Hermann, R., Knip, M., Veijola, R., Simell, O., Laine, A.-P., Åkerblom, H. K., … Ilonen, J. (2003). Temporal changes in the frequencies of HLA genotypes in patients with Type 1 diabetes—indication of an increased environmental pressure? *Diabetologia*, *46*(3), 420–425. https://doi.org/10.1007/s00125-003-1045-4

Higgins, C. (2015). Applications and challenges of digital pathology and whole slide imaging. *Biotechnic & Histochemistry*, *90*(5), 341–347. https://doi.org/10.3109/10520295.2015.1044566

Hyöty, H. (2016). Viruses in type 1 diabetes. *Pediatric Diabetes*, *17*, 56–64. https://doi.org/10.1111/pedi.12370

Hyöty, H., & Knip, M. (2014). Developing a vaccine for Type 1 diabetes through targeting enteroviral infections. *Expert Review of Vaccines*, *13*(8), 989–999. https://doi.org/10.1586/14760584.2014.933078

Isola, J., Tolonen, T., Tolonen, P., & Ylinen, O. (2016). Hematoxylin Counterstain To Simplify Whole Slide Scanning Of Immunofluorescence Stains. *Diagnostic Pathology*, *1*(8). https://doi.org/10.17629/www.diagnosticpathology.eu-2016-8:166

Kaufmann, S. H., Ewing, C. M., & Shaper, J. H. (1987). The erasable Western blot. *Analytical Biochemistry*, *161*(1), 89–95. https://doi.org/10.1016/0003-2697(87)90656-7

Knip, M., & Simell, O. (2012). Environmental triggers of type 1 diabetes. *Cold Spring Harbor Perspectives in Medicine*, *2*(7), a007690. https://doi.org/10.1101/cshperspect.a007690

Krogvold, L., Edwin, B., Buanes, T., Frisk, G., Skog, O., Anagandula, M., … Dahl-Jørgensen, K. (2015). Detection of a Low-Grade Enteroviral Infection in the Islets of Langerhans of Living Patients Newly Diagnosed With Type 1 Diabetes. *Diabetes*, *64*(5), 1682–1687. https://doi.org/10.2337/db14-1370

Krogvold, L., Edwin, B., Buanes, T., Ludvigsson, J., Korsgren, O., Hyöty, H., … Dahl-Jørgensen, K. (2014). Pancreatic biopsy by minimal tail resection in live adult patients at the onset of type 1 diabetes: experiences from the DiViD study. *Diabetologia*, *57*(4), 841–843. https://doi.org/10.1007/s00125-013-3155-y

Laitinen, O. H., Honkanen, H., Pakkanen, O., Oikarinen, S., Hankaniemi, M. M., Huhtala, H., … Hyoty, H. (2014). Coxsackievirus B1 Is Associated With Induction of -Cell Autoimmunity That Portends Type 1 Diabetes. *Diabetes*, *63*(2), 446–455. https://doi.org/10.2337/db13-0619

Laitinen, O. H., Svedin, E., Kapell, S., Nurminen, A., Hytönen, V. P., & Flodström-Tullberg, M. (2016). Enteroviral proteases: structure, host interactions and pathogenicity. *Reviews in Medical Virology*, *26*(4), 251–267. https://doi.org/10.1002/rmv.1883

Mao, Q., Wang, Y., Yao, X., Bian, L., Wu, X., Xu, M., & Liang, Z. (2014). Coxsackievirus A16: epidemiology, diagnosis, and vaccine. *Human Vaccines & Immunotherapeutics*, *10*(2), 360–367. https://doi.org/10.4161/hv.27087

Mebius, R. E., & Kraal, G. (2005). Structure and function of the spleen. *Nature Reviews Immunology*, *5*(8), 606–616. https://doi.org/10.1038/nri1669

Morel, P. A. (2013). Dendritic cell subsets in type 1 diabetes: friend or foe? *Frontiers in Immunology*, *4*, 415. https://doi.org/10.3389/fimmu.2013.00415

Murray, P. J., & Wynn, T. A. (2011). Protective and pathogenic functions of macrophage subsets. *Nature Reviews. Immunology*, *11*(11), 723–737. https://doi.org/10.1038/nri3073

Nagelkerke, S. Q., Bruggeman, C. W., den Haan, J. M. M., Mul, E. P. J., van den Berg, T. K., van Bruggen, R., & Kuijpers, T. W. (2018). Red pulp macrophages in the human spleen are a distinct cell population with a unique expression of Fc-γ receptors. *Blood Advances*, *2*(8), 941–953. https://doi.org/10.1182/bloodadvances.2017015008

Natkunam, Y. (2007). The biology of the germinal center. *Hematology. American Society of Hematology. Education Program*, *2007*(1), 210–215. https://doi.org/10.1182/asheducation-2007.1.210

Negoescu, A., Labat-Moleur, F., Lorimier, P., Lamarcq, L., Guillermet, C., Chambaz, E., & Brambilla, E. (1994). F(ab) secondary antibodies: a general method for double immunolabeling with primary antisera from the same species. Efficiency control by chemiluminescence. *The Journal of Histochemistry & Cytochemistry*, *42*(3), 433–437. https://doi.org/10.1177/42.3.7508473

Oikarinen, M., Laiho, J. E., Oikarinen, S., Richardson, S. J., Kusmartseva, I., Campbell-Thompson, M., … Hyoty, H. (2018). Detection of enterovirus protein and RNA in multiple tissues from nPOD organ donors with type 1 diabetes. *BioRxiv*, 459347. https://doi.org/10.1101/459347

Oikarinen, M., Tauriainen, S., Oikarinen, S., Honkanen, T., Collin, P., Rantala, I., … Hyoty, H. (2012). Type 1 Diabetes Is Associated With Enterovirus Infection in Gut Mucosa. *Diabetes*, *61*(3), 687–691. https://doi.org/10.2337/db11-1157

Oikarinen, S., Tauriainen, S., Hober, D., Lucas, B., Vazeou, A., Sioofy-Khojine, A., … Group, V. S. (2014). Virus Antibody Survey in Different European Populations Indicates Risk Association Between Coxsackievirus B1 and Type 1 Diabetes. *Diabetes*, *63*, 655–662. https://doi.org/10.2337/db13-0620

Pirici, D., Mogoanta, L., Kumar-Singh, S., Pirici, I., Margaritescu, C., Simionescu, C., & Stanescu, R. (2009). Antibody Elution Method for Multiple Immunohistochemistry on Primary Antibodies Raised in the Same Species and of the Same Subtype. *Journal of Histochemistry & Cytochemistry*, *57*(6), 567–575. https://doi.org/10.1369/jhc.2009.953240

Pugliese, A., Yang, M., Kusmarteva, I., Heiple, T., Vendrame, F., Wasserfall, C., … Atkinson, M. A. (2014). The Juvenile Diabetes Research Foundation Network for Pancreatic Organ Donors with Diabetes (nPOD) Program: goals, operational model and emerging findings. *Pediatric Diabetes*, *15*(1), 1–9. https://doi.org/10.1111/pedi.12097

Racaniello, V. R. (2006). One hundred years of poliovirus pathogenesis. *Virology*, *344*(1), 9–16. https://doi.org/10.1016/j.virol.2005.09.015

Ramos-Vara, J. A. (2005). Technical Aspects of Immunohistochemistry. *Veterinary Pathology*, *42*(4), 405–426. https://doi.org/10.1354/vp.42-4-405

Ramos-Vara, J. A. (2011). Principles and Methods of Immunohistochemistry. In *Methods in Molecular Biology* (Vol. 691, pp. 83–96). https://doi.org/10.1007/978-1-60761-849-2_5

Rhoades, R. E., Tabor-Godwin, J. M., Tsueng, G., & Feuer, R. (2011). Enterovirus infections of the central nervous system. *Virology*, *411*(2), 288–305. https://doi.org/10.1016/j.virol.2010.12.014

Richardson, S. J., Willcox, A., Bone, A. J., Foulis, A. K., & Morgan, N. G. (2009). The prevalence of enteroviral capsid protein vp1 immunostaining in pancreatic islets in human type 1 diabetes. *Diabetologia*, *52*(6), 1143–1151. https://doi.org/10.1007/s00125-009-1276-0

Robinson, S. M., Tsueng, G., Sin, J., Mangale, V., Rahawi, S., McIntyre, L. L., … Feuer, R. (2014). Coxsackievirus B Exits the Host Cell in Shed Microvesicles Displaying Autophagosomal Markers. *PLOS Pathogens*, *10*(4), e1004045. https://doi.org/10.1371/journal.ppat.1004045

Rojo, M. G., García, G. B., Mateos, C. P., García, J. G., & Vicente, M. C. (2006). Critical Comparison of 31 Commercially Available Digital Slide Systems in Pathology. *International Journal of Surgical Pathology*, *14*(4), 285–305. https://doi.org/10.1177/1066896906292274

Romijn, H. J., van Uum, J. F. M., Breedijk, I., Emmering, J., Radu, I., & Pool, C. W. (1999). Double Immunolabeling of Neuropeptides in the Human Hypothalamus as Analyzed by Confocal Laser Scanning Fluorescence Microscopy. *Journal of Histochemistry & Cytochemistry*, *47*(2), 229–235. https://doi.org/10.1177/002215549904700211

Saarinen, N. V. V., Laiho, J. E., Richardson, S. J., Zeissler, M., Stone, V. M., Marjomäki, V., … Laitinen, O. H. (2018). A novel rat CVB1-VP1 monoclonal antibody 3A6 detects a broad range of enteroviruses. *Scientific Reports*, *8*(1), 33. https://doi.org/10.1038/s41598-017-18495-4

Scalia, C. R., Gendusa, R., & Cattoretti, G. (2016). A 2-Step Laemmli and Antigen Retrieval Method Improves Immunodetection. *Applied Immunohistochemistry & Molecular Morphology*, *24*(6), 436–446. https://doi.org/10.1097/pai.0000000000000203

Schnell, S. A., Staines, W. A., & Wessendorf, M. W. (1999). Reduction of Lipofuscin-like Autofluorescence in Fluorescently Labeled Tissue. *Journal of Histochemistry & Cytochemistry*, *47*(6), 719–730. https://doi.org/10.1177/002215549904700601

Solomon, T., Lewthwaite, P., Perera, D., Cardosa, M. J., McMinn, P., & Ooi, M. H. (2010). Virology, epidemiology, pathogenesis, and control of enterovirus 71. *The Lancet Infectious Diseases*, *10*(11), 778–790. https://doi.org/10.1016/S1473-3099(10)70194-8

Spagnuolo, I., Patti, A., Sebastiani, G., Nigi, L., & Dotta, F. (2013). The case for virus-induced type 1 diabetes. *Current Opinion in Endocrinology & Diabetes and Obesity*, *20*(4), 292–298. https://doi.org/10.1097/med.0b013e328362a7d7

Steiniger, B. S. (2015). Human spleen microanatomy: why mice do not suffice. *Immunology*, *145*(3), 334–346. https://doi.org/10.1111/imm.12469

Steiniger, B. S., Seiler, A., Lampp, K., Wilhelmi, V., & Stachniss, V. (2014). B lymphocyte compartments in the human splenic red pulp: capillary sheaths and periarteriolar regions. *Histochemistry and Cell Biology*, *141*(5), 507–518. https://doi.org/10.1007/s00418-013-1172-z

Steiniger, B. S., Ulrich, C., Berthold, M., Guthe, M., & Lobachev, O. (2018). Capillary networks and follicular marginal zones in human spleens. Three-dimensional models based on immunostained serial sections. *PLOS One*, *13*(2), e0191019. https://doi.org/10.1371/journal.pone.0191019

Tauriainen, S., Salmela, K., Rantala, I., Knip, M., & Hyöty, H. (2010). Collecting high-quality pancreatic tissue for experimental study from organ donors with signs of β-cell autoimmunity. *Diabetes/Metabolism Research and Reviews*, *26*(7), 585–592. https://doi.org/10.1002/dmrr.1129

TEDDY Study Group. (2007). The Environmental Determinants of Diabetes in the Young (TEDDY) study: study design. *Pediatric Diabetes*, *8*(5), 286–298. https://doi.org/10.1111/j.1399-5448.2007.00269.x

Valnes, K., & Brandtzaeg, P. (1984). Paired indirect immunoenzyme staining with primary antibodies from the same species. Application of horseradish peroxidase and alkaline phosphatase as sequential labels. *The Histochemical Journal*, *16*(5), 477–487. https://doi.org/10.1007/BF01041348

Victora, G. D., & Nussenzweig, M. C. (2012). Germinal Centers. *Annual Review of Immunology*. https://doi.org/10.1146/annurev-immunol-020711-075032

Wang, W., Singh, S., Zeng, D. L., King, K., & Nema, S. (2007). Antibody Structure, Instability, and Formulation. *Journal of Pharmaceutical Sciences*, *96*(1), 1–26.

https://doi.org/10.1002/jps.20727
Whittington, N. C., & Wray, S. (2017). Suppression of Red Blood Cell Autofluorescence for Immunocytochemistry on Fixed Embryonic Mouse Tissue. *Current Protocols in Neuroscience*, *81*, 2.28.1-2.28.12. https://doi.org/10.1002/cpns.35
Wilkins, B. S., & Wright, D. H. (2000). Normal structure, development and functions of the spleen. In *Illustrated Pathology of The Spleen* (pp. 13–34). Cambridge: Cambridge University Press. https://doi.org/10.1017/CBO9780511545979.003
Writing Group for the TRIGR Study Group, W. G. for the T. S., Knip, M., Åkerblom, H. K., Al Taji, E., Becker, D., Bruining, J., … Wasikowa, R. (2018). Effect of Hydrolyzed Infant Formula vs Conventional Formula on Risk of Type 1 Diabetes: The TRIGR Randomized Clinical Trial. *JAMA*, *319*(1), 38–48. https://doi.org/10.1001/jama.2017.19826
Yarilin, D., Xu, K., Turkekul, M., Fan, N., Romin, Y., Fijisawa, S., … Manova-Todorova, K. (2015). Machine-based method for multiplex in situ molecular characterization of tissues by immunofluorescence detection. *Scientific Reports*, *5*(1), 9534. https://doi.org/10.1038/srep09534
Yeung, W.-C. G., Rawlinson, W. D., & Craig, M. E. (2011). Enterovirus infection and type 1 diabetes mellitus: systematic review and meta-analysis of observational molecular studies. *BMJ*, *342*, d35. https://doi.org/10.1136/bmj.d35
Zakerhamidi, M. S., Ahmadian, S. M. S., & Kian, R. (2015). The specific and nonspecific solvatochromic behavior of Sudan dyes in different solvents. *Canadian Journal of Chemistry*, *93*(6), 639–647. https://doi.org/10.1139/cjc-2014-0489
Zhang, Y., Wang, Y., Cao, W.-W., Ma, K.-T., Ji, W., Han, Z.-W., … Li, L. (2018). Spectral Characteristics of Autofluorescence in Renal Tissue and Methods for Reducing Fluorescence Background in Confocal Laser Scanning Microscopy. *Journal of Fluorescence*, *28*(2), 561–572. https://doi.org/10.1007/s10895-018-2217-4